12-2003

Classifying Forest Composition using Fractal Dimension as an Index of Image Texture

Fitria Latifah Wahid

CLASSIFYING FOREST COMPOSITION USING FRACTAL DIMENSION AS AN INDEX OF IMAGE TEXTURE

by

Fitria Latifah Wahid

A Thesis
Submitted to the
Faculty of The Graduate College
in partial fulfillment of the
requirements for the
Degree of Master of Arts
Department of Geography

Western Michigan University
Kalamazoo, Michigan
December 2003

ACKNOWLEDGMENTS

Alhamdulillah, I am finally able to finish this thesis. I wish to express my deepest appreciation and thanks to Dr. Charles 'Jay' Emerson, for all the extensive professional guidance, and continuous support. I am so grateful to have Jay as my advisor. To thank him, I do not even know where to begin. I also want to thank Dr. Lisa DeChano and Dr. James Biles, my thesis committee members, for their input, encouraging words, and motivation that helped me in finishing my thesis.

I would also like to recognize Dr. David Dickason and Greg Anderson, for the orthophoto of the Fort Custer Training Center, MI, used in this thesis, and also for the opportunity to work at the GIS Research Center during summer 2003. The experience and the technical training I received during that time, has proved to be very helpful in conducting my thesis research.

My gratitude is also extended to all graduate student colleagues at the Geography Department for their support, humor, and friendship. The same gratitude goes to the Indonesian society in Kalamazoo. I also want to thank J.P Marsch for his support and input throughout the time I was finishing this thesis.

Finally, I could not have gotten to this point if it were not for the incredible supports and love of my parents, my sister, my brother, and all my family in Indonesia. Thank you all for listening and giving me motivation throughout my education. I dedicate this thesis to you.

Fitria Latifah Wahid

CLASSIFYING FOREST COMPOSITION USING FRACTAL DIMENSION AS AN INDEX OF IMAGE TEXTURE

Fitria Latifah Wahid, M.A.

Western Michigan University, 2003

In this study, Landsat imagery from June (summer) and October (autumn senescence) 2000 of the area of Fort Custer Training Center in Kalamazoo and Calhoun Counties, Michigan, were analyzed for forest classification accuracies. The use of fractal analysis to improve forest classification, particularly to distinguish among northern hardwood species, was examined. Using moving windows with different sizes, measurement of local fractal dimension and spatial autocorrelation (Moran's I) were performed on the NDVIs and the panchromatic images. The measurement products were combined with Landsat TM bands as additional layers in supervised maximum-likelihood multispectral classifications. The accuracy for multispectral classification of the October scene is 43.21 percent. The addition of the fractal dimension measurement on the October panchromatic image results in 45.06 percent accuracy, showing a slight improvement of 1.85 percent. The accuracy for the multispectral classification of the June scene is only 30.25 percent. However, the fractal dimension seems to work better on the June scene, since it gives a higher percentage of improvement. The addition of fractal dimension measurements on the June NDVI and panchromatic image gives 36.42 percent of accuracy, an improvement of 6.17 percent compared with using the spectral bands alone.

TABLE OF CONTENTS

Table of Contents—continued

Table of Contents—continued

LIST OF TABLES

LIST OF FIGURES

List of Figures—Continued

CHAPTER I

INTRODUCTION

Forests are home to organisms at the surface of the earth and provide multiple benefits for them, including habitat for flora and fauna, maintenance of air, soil and water, opportunities for recreation, and economic benefits from timber. To preserve the benefits that forests provide, a sustainable forest management is required.

Sustainable forest management entails the knowledge of forest structure, composition, and diversity. To acquire this knowledge, forest inventory is usually performed. Forest inventory is defined as an assessment of forest resources which describes the location and nature of forest cover, including tree size, age, volume, and species composition (National Community Forestry Center Northern Forest Region, 2003). Traditional or conventional forest inventory involves ground survey of the forested area to collect information. This method of forest inventory usually produces accurate results, even though it necessitates a lot of time and cost to conduct.

As an alternative to performing the conventional method, the use of remotely sensed data has been recognized in forest inventory. The application of spectral analysis on satellite imagery for forest cover type mapping has been utilized primarily for delineating forest areas from other land use/ land cover, and also for discriminating between deciduous and conifer trees. The accuracy assessment of forest classification at these levels using the multispectral approach has been reported as acceptable (Bolstad and Lillesand, 1992; Gerylo et al, 1998; Hudson, 1987; Hoffer, 1990; Moskal and Franklin, 2001).

However, in any sustainable forest management program, information on these levels is not enough. More detailed information on species composition at species group or species association level is needed to support decision making in the forest management program. Unfortunately, the accuracy of the automated forest classification for species group level is still relatively poor, especially for the northern Lake States region (Mladenof and Host, 1994). Similar spectral characteristics shown by different species makes it hard to distinguish among species, especially hardwood species. Hence, another classification method that does not solely depend on spectral characteristics of features in the images might be more accurate.

Traditional spectral analysis of remotely sensed images, which is applied on a pixel by pixel basis, ignores the potentially useful spatial information between the values of proximate pixels (Atkinson and Tate, 2000). One way to overcome this problem is to improve the classification result of the images through spatial pattern recognition using other image interpretation elements such as texture.

There are many possible texture measures of an image, one of which is through fractal analysis. Fractals are geometrical figures with irregular and fragmented patterns in nature (Mandelbrot, 1982). One of the properties that a fractal form (can be a point, a curve, or a surface) possesses is self-similarity. With this self-similarity property, the nature form is invariant with respect to scale (Goodchild, 1980).

Mladenoff and Host (1994) described four general application areas for remote sensing and GIS in the Lake States regions: (1) forest and land cover mapping, (2) ecological land classification, (3) regional change detection, and (4) detection and modeling of ecosystem properties and processes. This study is an effort to address the

application area of the use of remote sensing and GIS in forest and land cover mapping in the northern Lake States, particularly in Michigan. The problem that this study is attempting to confront is the difficulty in classifying forest composition at species group level precision using Landsat images in the region. The study will examine the use of fractal analysis to improve forest classification accuracy. The objective of the study is to determine the effectiveness of fractal analysis when combined with the multispectral approach using a supervised maximum likelihood classifier in forest classification and species differentiation, with an emphasis in distinguishing among northern hardwood species, particularly oak species, in an area of southwestern part of Michigan.

The remainder of the thesis is designed in the following order: Chapter II will discuss the literature on image analysis, including spectral and spatial analysis, and accuracy assessment. Chapter III discusses the literature on Image Texture. Included in this chapter are texture measures methods, fractals and fractal dimension, and methods to calculate fractal dimension of an image. Chapter IV discusses the literature on forest classification, including methods that have been utilized in classifying forests using remotely sensed data. Chapter V will reveal the methodology used in the study. Chapter VI will disclose the results of the study, followed by the discussion; and finally. Chapter VII is the conclusion chapter.

CHAPTER II

IMAGE ANALYSIS

Overview

Image classification is a way to extract information from remotely sensed data (Jensen, 1996). In the process, each pixel is assigned to a class in the classification scheme. Classification schemes are a means of organizing spatial information in an orderly and logical way. A classification scheme has a set of labels and a set of definitions for assigning labels. It also has to be mutually exclusive and totally exhaustive, meaning that each pixel can only be assigned to one class. Sometimes, it is possible to have a class of unclassified pixels. The level of detail in the scheme influences the time and the effort needed to conduct the accuracy assessment (Congalton and Green, 2001).

In working with remotely sensed data, it is important to have a standardized framework of a classification scheme, to ensure uniformity in the categorization process among different studies or different works. Several classification systems have been established for use with remote sensing techniques. The Anderson classification system (Anderson et al, 1976) is the most widely accepted, especially in land cover classifications. Anderson levels increase in categorical detail with increasing level designation (Table 1). Land use/land cover data at Anderson level I and level II suit for planning purposes, however, greater accuracy or higher level data is required for regulation of land use activities (Anderson et al, 1976).

Table 1. Level I and Level II of the Anderson Classification System

Level I	Level II
1. Urban or Built-up Land	11. Residential 12. Commercial and Services 13. Industrial 14. Transportation, Communication, and Utilities 15. Industrial and Commercial Complexes 16. Mixed Urban or Built-up Land 17. Other urban or Built-up Land
2. Agricultural Land	21. Cropland 22. Orchards, Groves, Vineyard, Nurseries, and Ornamental Horticultural areas 23. Confined Feeding Operations 24. Other Agricultural Land
3. Rangeland	31. Herbaceous Rangeland 32. Shrub and Brush Rangeland 33. Mixed Rangeland
4. Forest Land	41. Deciduous Forest Land 42. Evergreen Forest Land 43. Mixed Forest Land
5. Water	51. Streams and Canals 52. Lakes 53. Reservoir 54. Bays and Estuaries
6. Wetland	61. Forested Wetland 62. Nonforested Wetland
7. Barren Land	71. Dry Salt Flats 72. Beaches 73. Sandy Areas other than Beaches 74. Bare Exposed Rock 75. Strip Mines, Quarries, and Gravel Pits 76. Transitional Areas 77. Mixed Barren Land
8. Tundra	81. Shrub and Brush Tundra 82. Herbaceous Tundra 83. Bare Ground Tundra 84. Wet Tundra 85. Mixed Tundra
9. Perennial Snow or Ice	91. Perennial Snowfields 92. Glaciers

Source : Anderson, et al., 1976

The process of assigning pixels or features to categories in the classification scheme can be based on different aspects, such as pixels' spectral characteristics or spatial characteristics. Time is also an important aspect in aiding in feature identification (Lillesand and Kiefer, 2000). All of these aspects would determine the procedure or algorithm to use in the classification process.

Spectral Analysis

Spectral analysis, which is also referred to as spectral pattern recognition, is the most used method in image classification. With this method, the assignment of each pixel to a class is determined by its spectral value. In spectral pattern recognition, one can perform an image classification using supervised and unsupervised approaches. The basic difference between the two methods is that supervised classification involves a training step followed by a classification step, whereas unsupervised classification performs the classification step using the natural spectral groupings, or clusters, and is then followed with the interpretation of these spectral clusters by the image analyst (Lillesand and Kiefer, 2000). Although not as popular, other approaches such as fuzzy logic classification and hybrid approaches involving the use of ancillary information can also be used in performing image classification (Jensen, 1996). The use of these methods depends on the nature of the data being used and important considerations that must be addressed in the research.

Unsupervised Classification

Unsupervised classification is also called clustering, because it is based on the

natural groupings of the spectral properties of pixels in multispectral feature space (ERDAS, 2002). The concept behind this method is that values within a given class should be close together in the measurement space, whereas data in different classes should be comparatively well separated (Lillesand and Kiefer, 2000). The method requires a minimum amount of initial input from the analyst. The analyst must determine the number of classes desired, and after the data is classified, he/she must use his/her interpretation skill to determine what feature or classes of interest associate with the classified spectral classes.

A widely used clustering algorithm in unsupervised classification is the Iterative Self-Organizing Data Analysis Technique (ISODATA). ISODATA represents a fairly comprehensive set of heuristic procedures that have been incorporated into an iterative classification algorithm (Jensen, 1996). ISODATA is iterative because it makes a large number of passes through the dataset until specified results are attained. To perform ISODATA clustering, the number of clusters considered, the maximum number of iterations, and a convergence threshold need to be specified. The convergence threshold is the maximum percentage of pixels whose cluster assignment can go unchanged between iterations (ERDAS, 2002).

Supervised Classification

In supervised classification, the image analyst specifies numerical descriptors of the classes of interest in a scene. This is done by building training areas, which are representative sample sites of known classes, to describe the spectral attributes for each feature type or class of interest (Lillesand and Kiefer, 2000).

Building training areas that adequately represent the classes in the classification scheme is important because it will determine the accuracy of the classification. Hence, a priori knowledge of the scene being classified is required to get the desired training sets. All spectral classes constituting each information class must be adequately represented in the training set statistics used to classify the scene (Lillesand and Kiefer, 2000). The theoretical minimum limit of the number of pixels that must be contained in a training set is n + 1, where n is the number of bands. Once the training sets have been collected, a decision has to be made to determine the bands that are most effective in discriminating each class from all others (Jensen, 1996).

Several algorithms are available to perform the supervised classification on an image. One simple algorithm is called the Minimum-Distance-to Means Classifier. With this algorithm, a pixel may be classified by computing the distance between the value of the unknown pixel and each of the category means, which have been determined previously (Lillesand and Kiefer, 2000). In Figure 1a, the category means are indicated by +'s in the gray little boxes, while the unknown pixels are indicated by point 1 and 2. After the distances are computed, the pixel is assigned to the closest class (Figure 1b). If the pixel is farther than the defined distance from any category mean, it would be classified as unknown.

Another commonly used algorithm for supervised classifications is called the Maximum Likelihood Classifier. This algorithm is based on the probability that a pixel belongs to a particular class (ERDAS, 2002). The basic equation assumes that these probabilities are equal for all classes, and that the input bands have normal distributions.

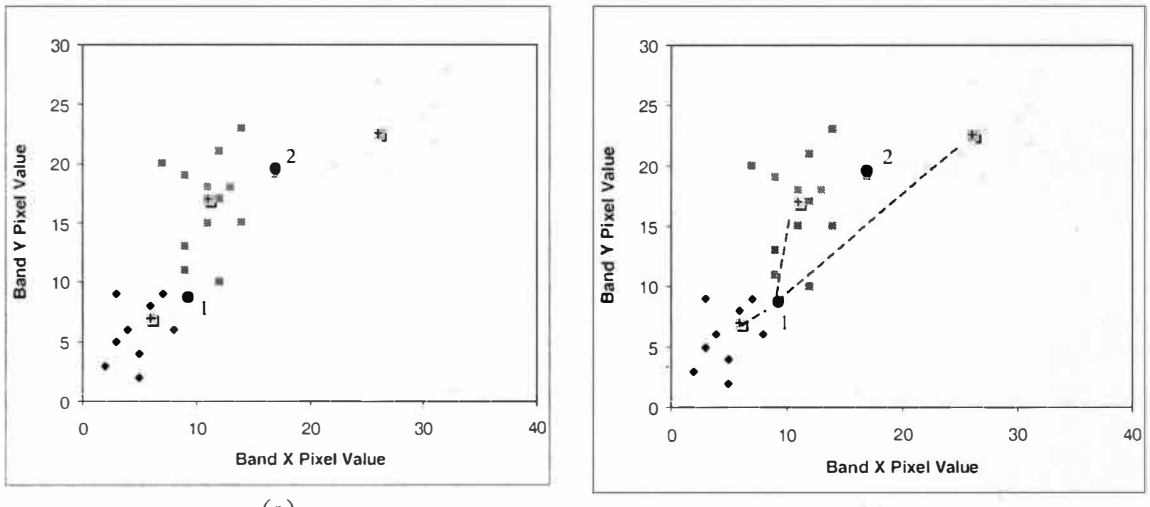

Figure 1. Minimum Distance to Means Classifier

Under this assumption, the distribution of a category response pattern can be described by the mean vector and the covariance matrix. The probability value of a given pixel value can be plotted in a three dimensional graph, with the vertical axis indicating the probability of a pixel value being a member of one of the categories. The resulting bell-shaped surfaces are called *probability density functions* (Lillesand and Kiefer, 2000). After evaluating the probability in each category, the pixel would be assigned to the most likely class (highest probability value).

The maximum likelihood classifier can also be described in a scatter diagram. In the diagram, the classifier delineates ellipsoidal 'equiprobability contours', where the shape of the contours expresses the sensitivity of the likelihood classifier to covariance (Figure 2).

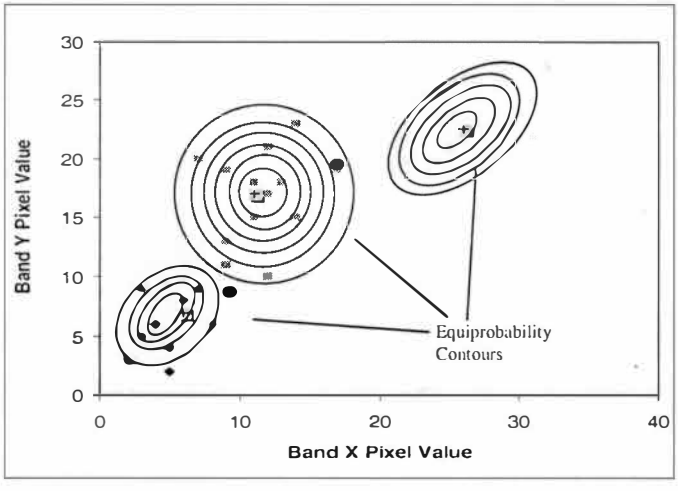

Figure 2. Equiprobability Contours

Accuracy Assessment

Regardless of the method being used, after the classification result is derived, an accuracy assessment is needed to determine the quality of the classified data or map produced, by identifying and correcting the errors. In performing accuracy assessment, the remote-sensing- derived classification maps are compared to reference test information or reference data (Jensen, 1996), and calculations are made to determine how close the classification map is from the truth, represented by the reference data.

Ideally, reference data for accuracy assessment should be collected as close as possible to the date of the collection of the remotely sensed data used to make the map (Congalton and Green, 2001). However, it is not always possible to do so, considering the time and the cost needed. In either case, it is important to keep the accuracy reference data independent of any training data to ensure objectivity and consistency of the results.

One of the most common means to report classification accuracies is by using a classification error matrix (also called confusion matrix or contingency table) (Lillesand

and Kiefer, 2000). An error matrix is a square array of numbers set out in rows and columns that express the number of sample units (pixels, clusters, or polygons) assigned to a particular category in one classification relative to the number of sample units assigned to the same category in another classification (Congalton and Green, 2001).

Information in the error matrix may be calculated using simple descriptive statistics or discrete multivariate analytical statistical techniques. An error matrix is a very effective way to represent map accuracy in that the individual accuracies of each category are described along with both the errors of inclusion (commission error) and errors of exclusion (omission errors) (Congalton and Green, 2001). A commission error happens when an area or pixel that does not belong to a category is included in that category, and an omission error occurs when an area or pixel is not included in a category where it belongs.

The probability of any class being classified is indicated by the overall accuracy (Gonzales, 1994) and simply retrieved from the sum of the major diagonal (the correctly classified sample units) divided by the total number of sample units in the entire error matrix. Instead of only representing the overall classification accuracy, the individual category accuracies can be described using the producer's and the user's accuracies. The producer's accuracy is achieved by dividing the total number of correct sample units in a particular category by the total number of sample units in that category as indicated by the reference data. This parameter quantifies how well a particular characteristic or class can be mapped. The user's accuracy indicates how reliable the map is from the user's standpoint or how well the map represents what is actually on the ground (Gonzales, 1994). The user's accuracy is calculated by dividing the total number of correct sample

units in a particular category by the total number of sample units classified as that category (Congalton and Green, 2001).

The KHAT statistic or the Cohen's Kappa value is another commonly used measure of agreement or accuracy (Cohen, 1960; Congalton and Green, 2001). The Cohen's Kappa or Kappa value measure is based on the difference between the actual agreement in the error matrix and random agreement. The Kappa index ranges between 0 and 1 and expresses the proportionate reduction in error achieved by a classifier as compared with the error of a completely random classifier. For instance, a Kappa value of 0.75 would indicate that the classifier was avoiding 75 percents of the errors that a totally random process would have produced (Lillesand and Kiefer, 2000).

Spatial Analysis

Besides using spectral characteristics of the pixels in an image, spatial pattern recognition may also be used to classify the image. Spatial pattern recognition involves the categorization of image pixels on the basis of their spatial relationship with pixels surrounding them. To recognize the spatial pattern of an image, one can perform spatial filtering, which is an operation where pixel values in an original image are modified on the basis of the gray levels of neighboring pixels (Lillesand and Kiefer, 2000). The most widely used method of spatial filtering is known as convolution, which involves passing a square window (also called as a moving window, a kernel or a filter) over the image. Moving windows are defined in part by their dimension, where odd numbers are used most of the time (e.g 3x3, 5x5, etc) (Bolstad, 2001). Figure 3 shows the concept of moving window.

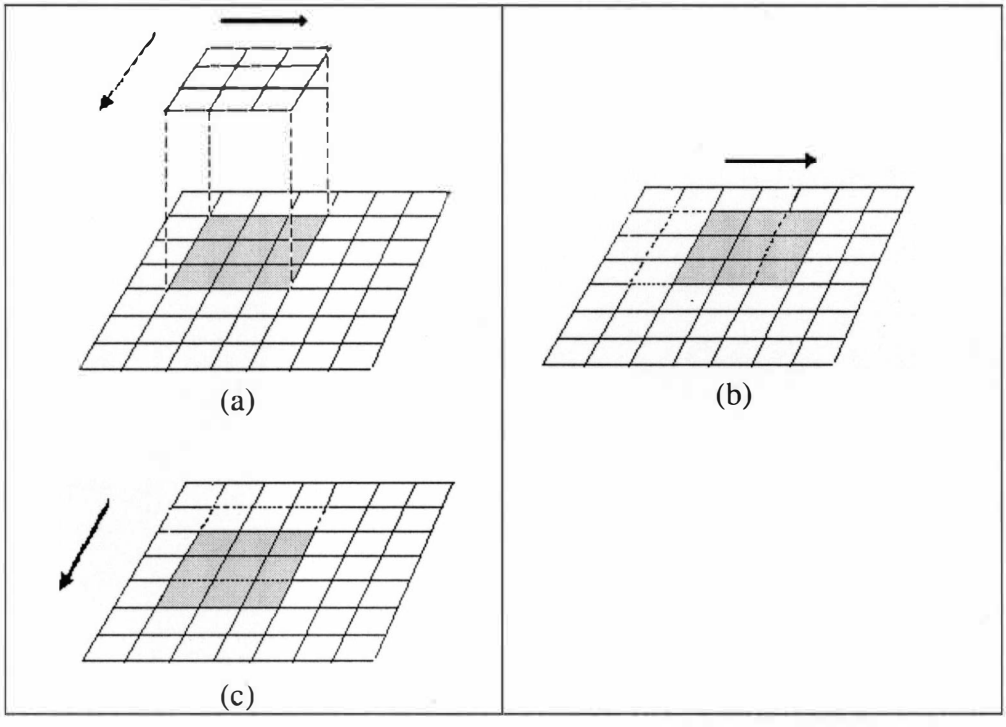

Legend. (a) A moving window covers three rows and three columns of pixels (3x3)
(b) The moving window moves along a line to cover another 3 x 3 pixels
(c) The moving window continues to move from line to line

Figure 3. The Concept of Moving Window

A new value for the central cell of the window $C_{i,j}$ can be computed as a function of the cell values covered by the window (Burrough and McDonnel, 2000). The general equation for performing a convolution is :

$$C_{ij} = f\left(\sum_{i-m}^{i+m}\sum_{j-n}^{j+n} C_{ij}.\lambda_{i,j}\right) \qquad [1]$$

where i, j = position of pixel (row, column)

f = a given window operator on windows of sides 2m+1, 2n+1

$\lambda_{i,j}$ = a weighting factor

C_{ij} is usually computed (using window operator f) as simple arithmetic average of the values of the other cells. Some arithmetic operations that can be applied in a moving window include finding range, diversity, total, minimum, mean, maximum, mode, and standard deviation (Burrough and McDonnell, 2000). Figure 4 shows one of these arithmetic operations.

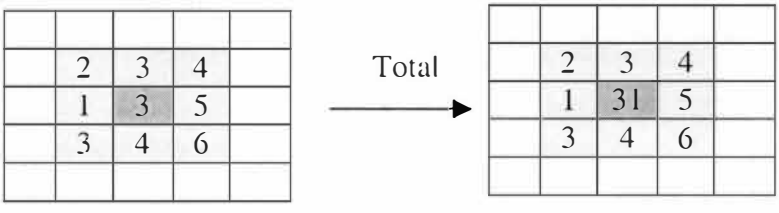

Figure 4. An Arithmetic Operation for Spatial Filtering

A spatial classifier might consider aspects that humans synergistically take into account in a visual classification process, such as image texture, context, edges, pixel proximity, feature size, shape, directionality, and tonal variation (Lillesand and Kiefer, 1987). From all of the elements above, texture has been the aspect that receives the most attention in remote sensing research (Jaggi et al., 2003; Jakubauskas, 1997; Moskal and Franklin, 2001; Moskal and Jakubauskas, 2001; Hay et al., 1996; Arumugam et al., 2003).

CHAPTER III

IMAGE TEXTURE

Texture Measures

Image texture is defined as the spatial variation in image tones, and several attempts have been made to try to incorporate texture into the classification process by creating a new texture image that can be used as another feature or band in the classification (Jensen, 1996). Most existing texture recognition approaches can be broken down into components which are based on statistical (Jakubauskas, 1997), structural properties of the image (Keller et al., 1989), spectral components (Haralick et al., 1973), and the manipulation of the spatial frequency within an image (Lillesand and Kiefer, 2000). Statistical methods yield characterizations of textures such as smooth, rough, etc. through a quantitative assessment. Structural techniques examine the arrangement of landscape patterns in an image, which include the distinction between human induced physical changes and those of naturally occurring processes. Spectral features are used to describe the average tonal variations in various bands (Haralick et al., 1973).

There are a number of possible approaches that can be used in texture measurement of an image. Some approaches are texture features based on first-order statistics; second-order gray level statistics; Fourier analysis; and fractal analysis.

First-Order Statistics

First-order statistic is the smallest observation in a sample. Texture measures based on this method use first-order statistics of local areas, such as means, variance, standard deviation, and entropy. The use of these statistical parameters to aid in image classification has been evaluated, and it has been found that the standard deviation measure was the best to use (Jensen, 1996). However, the use of standard deviation is not as effective as the use of the gray level value co-occurrence matrix.

Second Order Statistics/Gray Level Co-Occurrence Matrix

Haralick et al. (1973) developed the gray level co-occurrence matrix (GLCO), which is based upon repeated occurrences o f gray level patterns in an image. This method involves the use of arrays termed angular nearest neighbor gray-tone spatial dependence matrices for the measurement of texture (Figure 5). The matrices that are created are a function of the angular relationship between neighboring pixels as well as a function of the differences between them.

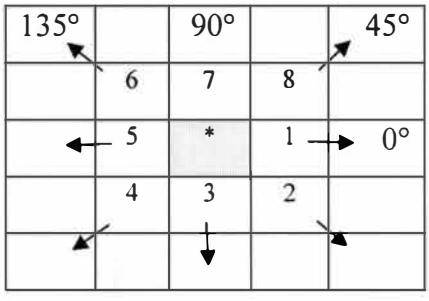

Figure 5. Angular Nearest Neighbor Gray-tone Spatial Dependence Matrix

Texture patterns then can be detected by calculating the relative frequencies at which two neighboring pixel cells are separated by a given distance on an image. It is assumed that all textural information is contained in the brightness or gray level value spatial-dependency matrices that are developed for angles of 0°, 45°, 90°, and 135° (Jensen, 1996).

If $c = (\Delta x, \Delta y)$ is considered a vector in the (x, y) image plane, for any such vector and for any image f(x, y) it is possible to compute the joint probability density of the pairs of brightness values that occur at pairs of points separated by c. The joint density takes the form of an array h_c, where h_c (i,j) is the probability that the pairs of brightness values (i,j) occur at separation c. From Figure 6, if $(\Delta x, \Delta y) = (1,0)$, then the numbers below are represented by the brightness value spatial-dependency matrix h_c:

Original Image =

0	1	1	2	3
0	0	2	3	3
0	1	2	2	3
1	2	3	2	2
2	2	3	3	2

h_c =

	0	1	2	3
0	1	2	1	0
1	0	1	3	0
2	0	0	3	5
3	0	0	2	2

Figure 6. Simplified Image of Gray Level Co-Occurrence Matrix

where the entry in row *i* and column *j* of the matrix is the number of times brightness value *i* occurs to the left of brightness value *j* (Jensen, 1996). For example, brightness value 1 is to the left of brightness value 2 a total of tree times or it can be written as h_c (1,2) = 3.

There are a variety of measures used to extract useful information from the matrices. Some of the widely used ones are the angular second moment (ASM), contrast, and correlation.

Fourier Analysis

Fourier analysis involves examining the frequency domain of an image by separating it into various spatial frequency components. The examination is completed through a mathematical operation application, known as the Fourier transform (Lillesand and Kiefer, 2000). A Fourier transform is a linear transformation that allows calculation of the coefficients necessary for the sine and cosine terms to adequately represent the image (ERDAS, 2002). Conceptually, the Fourier transform operates by fitting a continuous function through the discrete digital number values of an image as if they were plotted along each row and column

Fourier analysis is typically used for spatial filtering and the removal of noise. It is possible to perform what is known as a wedge block filter either in the horizontal or vertical direction (Lillesand and Kiefer, 2000). The filter allows interpreters to take an original image with significant horizontal noise, and generate a transform that would likely show a band of frequencies tending in the vertical direction.

Fractals

First introduced by Mandelbrot (1977, 1982), the concept of fractals is referred to as a family of shapes with irregular and fragmented patterns in nature. Mandelbrot (1977) defined fractals as a set for which the Haussdorff Besicovitch dimension strictly

exceeds the topological dimension. Topological dimension is described as the number of distinct coordinates needed to specify a position on or within an object (Xia and Clarke, 1997). In Euclidian space, a point has a topological dimension of zero, a line has a dimension of one, an area has two dimensions, and a volume has three dimensions.
A key functional concept of fractal analysis is self-similarity (Mandelbrot, 1982), which is defined as a property of a curve or a surface where each part is distinguishable from the whole, or where the form of the curve or surfaces is invariant with respect to scale (Goodchild, 1980).

There has been strong interest in the use of fractal analysis to characterize remotely sensed data, and the applications associated with spectral and spatial analysis of the data (Clarke, 1986; De Cola, 1989; Jaggi et al., 1993; Emerson et al., 1998; Caird, 2001). Fractal analysis provides tools for measuring how the geometric complexity of imaged objects changes when the image resolution is altered (Quattrochi et al., 2001).

One limitation of Euclidian or classical geometry is the lack of ability to analyze spatial patterns of nature, such as curves and surfaces. In Euclidian geometry, the topological dimensions are expressed with integer values and remain constant despite the complexity of the features. The fractal dimension (D) is a non-integer value expressing the degree of irregularity of a fractal form (Atkinson and Tate, 2000). Fractal dimension can be used to describe length, surface, and volume of most natural objects.

Unlike Euclidian geometry, lines, area and volume of natural objects are independent of the measurement unit (Mandelbrot, 1982; Zeide, 1991). The fractal dimension of a point pattern can be any real number between zero and one. Meanwhile, a curve or a line has a fractal dimension between one and two, depending on its

irregularity. The more contorted the straight line becomes the more space it fills within the box (Caird, 2001). A surface can have a fractal dimension between two and three. Increasing the geometrical complexity of a perfectly flat surface with a fractal dimension of 2.0, causes the surface to fill a volume, resulting in fractal dimension value approaching 3.0 (Quattrochi et al., 2001).

The complexity of images has been the reason why less attention is given to spatial analysis as compared to spectral analysis in digital image processing. Fractal dimension offers insight towards understanding texture in the spatial as well as spectral context of an image (Mandelbrot, 1982). Thus, fractal analysis could be applied to help in answering questions relating to real world phenomena.

Fractal Applications in Forestry

The use of fractal analysis has been reported in several studies, some of which are forestry related. Zeide (1991) mentioned that fractal geometry may produce methods for estimating stand density, predicting forest succession and describing the form of trees. He argued that the fractal dimension of tree crowns is a good indicator of various tree and site features such as species tolerance, crown class and site quality. Fractal analysis can also be used to understand landscape structure, as in assessing the fragmentation of forests. Landscape pattern, which refer to the measurement of terrain patches resulting from the fragmentation, provide a set of indicators that can be used to assess ecological status and trends at a variety of scales (Jensen, 2000).

Fractals have also been used for assessing a range and distribution of any given species. Virkkala (1992) studied the spatial distribution and the range of Northern Forest

Passerine birds using fractal analysis on different scales of resolution. The use of fractal geometry also can be found in studies of the effect of forest fires. Zhu et al (2000) argued that forest fire spread is self similar, since every fire point can ignite the combustibles around it, and the burning combustibles can be taken to leeward to ignite a new fire, which in turn leads to self-similarity to some extent.

Fractal Dimension as an Index of Image Texture

One way of estimating the fractal dimension value of a curve is to measure the length of the curve using various step sizes. The more irregular the curve, the increase in length is greater as step size decreases. Fractal dimension D can be calculated with the following equations:

$$Log L = K + B \log \delta \qquad [2]$$

$$D = 1 - B \qquad [3]$$

where:

L = length of the curve

δ = step size

B = slope of the regression

K = a constant

The fractal dimension value of a surface can be computed in a similar fashion through several methods. Three methods that have been applied to real data and documented in various studies are the variogram, the isarithm, and the triangular prism

(Lam and De Cola, 1993; Jaggi et al.; 1993; Xia and Clarke, 1997). These methods utilize the fractal dimension as an index of image texture.

Variogram

The variogram method uses the variogram function to measure the fractal dimension. This method has been used significantly in *kriging*, a spatial interpolation technique (Lam and De Cola, 1993). The variogram function describes how the surface heights between data points vary with their spatial distance. To calculate the variance for all data pairs that fall into a specified distance interval, *r(d)*, or lag, the following equation may be used:

$$\gamma(d) = \left(1/2\, n\right) \sum_{i=1}^{n} \left[z_i - z_{(d+1)}\right]^2 \qquad [4]$$

where:

n = total number of data pairs that fall in distance interval d

z = surface value

The semi-variances are then plotted against distances in double log form (Figure 7) (Lam et al., 2002). The fractal dimension D then can be estimated from the slope *b* of linear regression performed between semi-variances and distances with:

$$D = 3 - \left(b/2\right) \qquad [5]$$

Lam and De Cola (1993) mentioned the advantages and the disadvantages to using the variogram method. The advantage is that the method can be used upon samples of regular and irregular grid data to increase processing speed, and method would be

useful for measuring a fractal surface with low dimension. The major disadvantage is that it may not be appropriate for complex images because it tends to yield high fractal dimension values (Lam et al., 2002), which can be greater than 3.0. The other disadvantage of the variogram is that it is not appropriate for detecting scale ranges within images and it is also computationally intensive.

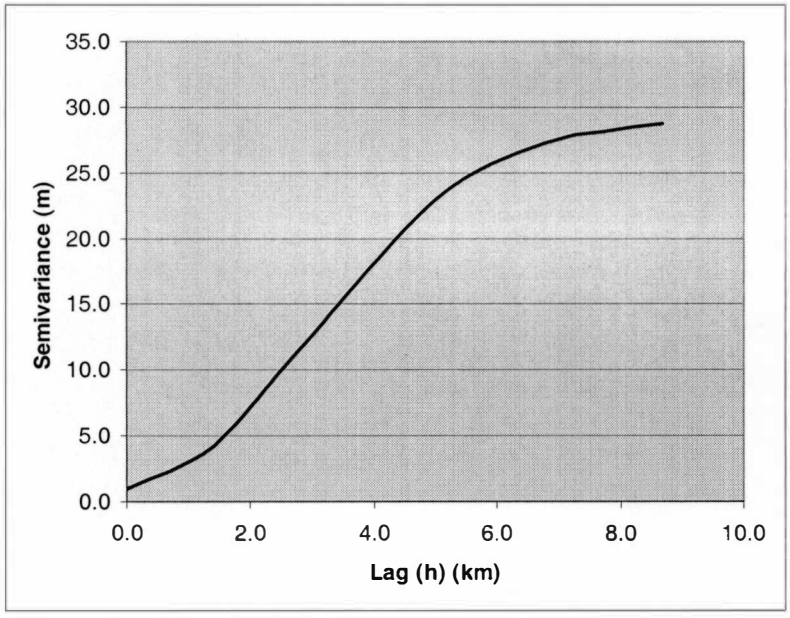

Figure 7. The Variogram

Isarithm

The isarithm method computes a mean fractal dimension from the individual D values of grey-scale contours. For each isarithm value and each step size, the algorithm classifies each pixel below the isarithm value as white and each pixel above it as black (Quattrochi et al., 2001). Step sizes are defined by units of grids that proceed by the number of grids (1, 2, 4, 8, etc.) (Lam and De Cola, 1993). Neighboring pixels along a row or a column then are being compared to examine if they are either both black or both

white. If they are dissimilar, it implies that an isarithm lies between the two neighboring pixels, which are then recorded as boundary pixels. The length of each isarithm line is approximated by using the total number of boundary pairs (Lam and De Cola, 1993; Caird, 2001). The total length of the boundary for each isarithm is plotted against step size in double log form. Fractal dimension of the isarithm line is determined by using the regression slope b, where:

$$D = 2 - b \qquad [6]$$

The fractal dimension of the surface is the average of the fractal dimension values for those isarithms with $R^2 \geq 0.9$. The arbitrary R^2 choice was made to help limit the inputs to the computation of fractal dimension to those isarithms that exhibit self-similarity (Lam and De Cola, 1993; Quattrochi et al., 2001). The reason for this is in the real word, fractal dimension of an image only applies over a certain scale, and the use of the arbitrary R^2 helps to ensure that the fractal dimension measures are within this scale.

Triangular Prism

Another method to measure fractal dimension of a surface was introduced by Clarke (1986). From Figure 8, if the four points of the corner of a grid are depicted by points E, F, G, and H; and points A, B, C, and D are corresponding with the height of z values of the grid corners, then a vertical line can be drawn, connecting the center point of the grid O with M, whose new value obtained by interpolation of the z values of the four corners (AE, BF, CG, and DH). Subsequently, four triangular prisms can be drawn by connecting each corner to the center point (MA, MB, MC, and MD). Figure 9 shows the top view of pixel with side s.

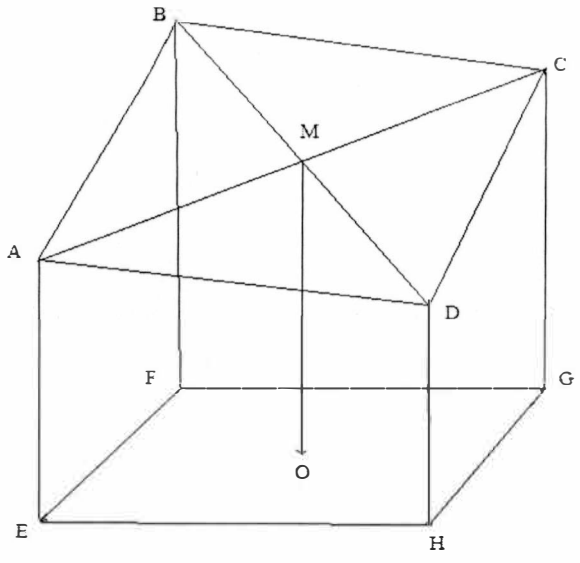

Figure 8. Three Dimensional Triangular Prism Method

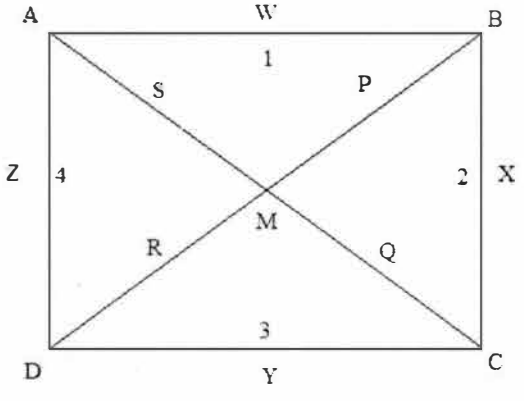

Figure 9. Top View Calculation of Triangular Prism Method

If the diagonals of the prisms have a length of $\sqrt{2}2s$, the length of sides of the upper face of the prism can be obtained using Pythagoras' theorem, considering the height differences between corners.

$$W = \sqrt{(B-A)^2 + s^2} \qquad X = \sqrt{(C-B)^2 + s^2}$$

$$Y = \sqrt{(D-C)^2 + s^2} \qquad Z = \sqrt{(A-D)^2 + s^2} \qquad [7]$$

$$S = \sqrt{(A-C)^2 + \left(\sqrt{2}/2s\right)^2} \qquad P = \sqrt{(B-M)^2 + \left(\sqrt{2}/2s\right)^2}$$

$$Q = \sqrt{(C-M)^2 + \left(\sqrt{2}/2s\right)^2} \qquad R = \sqrt{(D-M)^2 + \left(\sqrt{2}/2s\right)^2} \qquad [8]$$

Then, the surface area of the triangles can be computed using Heron's formula (Clarke, 1986).

$$sA = 1/2(W + P + S) \qquad sB = 1/2(X + P + Q)$$

$$sC = 1/2(Y + Q + S) \qquad sD = 1/2(Z + S + R) \qquad [9]$$

The areas of four triangles 1, 2, 3, and 4:

$$1 = \sqrt{sA(sA - W)(sA - P)(sA - S)}$$

$$2 = \sqrt{sB(sB - X)(sB - P)(sB - Q)}$$

$$3 = \sqrt{sC(sC - Y)(sC - Q)(sC - R)}$$

$$4 = \sqrt{sD(sD - Z)(sD - S)(sD - R)} \qquad [10]$$

The total surface area for the prism can be computed by adding the areas for triangles 1, 2, 3, and 4.

$$\text{Total surface area for prism} = 1 + 2 + 3 + 4 \qquad [11]$$

The measurement of the prism surface area can be started from the center of the moving window used. From Figure 10 a, in a 9x9 window, the surface area is calculated for the yellow prism, using the average height of the four gray pixels for the height (z value) of the center point. The step is then repeated using incremented grid size within the moving window. In this next step (figure 10 b), the surface area for the prism is again

calculated, but this time the height of each corner of the grid used in the area measurement is the average of heights of four colored pixels. The height of the center point of the grid is then calculated by averaging the heights at four corners of the grid, and the prism area is calculated subsequently. The step is again repeated until all pixels in the moving window are covered by the increment. The use of a 9x9 window would result in four different grid sizes.

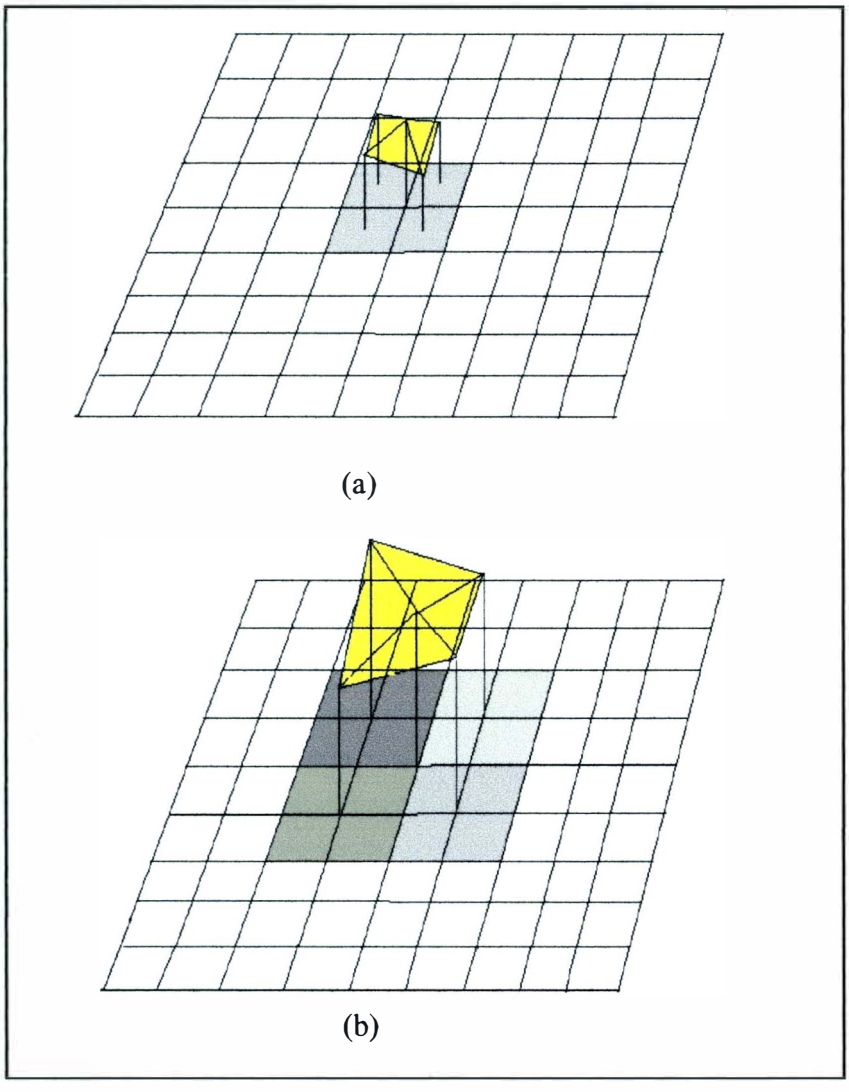

Legend. (a) Step 1 (b) Step 2

Figure 10. Triangular Prism Method in a 9x9 Moving Window

By performing a log-log regression of grid sizes with the prism areas, the relationship between the total area of the surface and the grid sizes is obtained. With the 9x9 window example, there would be four points plotted on the regression line. The fractal dimension then is calculated as 2 – b, where b is the slope of the line from the regression (Clarke, 1986). The triangular prism method is used to compute the fractal dimension of entire images (Clarke, 1986; Jaggi et al., 1993), meaning that it would produce one measurement of fractal dimensions for a whole image or specified subsets of an image.

Local Fractals and ICAMS

Local fractal dimensions are a series of values determined within an overlapping or non-overlapping moving window. After specifying a square window having an odd number of pixels on each side, the triangular prism method is used to calculate the fractal dimension for the central pixel in the moving window. The moving window is then passed throughout the image, and calculation is repeated on every window location across the image, where the fractal dimension is used as the pixel value of the new output image. The new output image will then contain a set of fractal dimensions.

Quattrochi et al. (1997) have developed a software module called ICAMS (Image Characterization and Modeling System), which is intended to measure, characterize and model multi-scale remotely sensed data (Quattrochi et al., 2001). ICAMS contains a number of spatial measurement methods and it is designed to run on Intergraph-MGE and ArcInfo platforms, and also to run as a stand-alone application. ICAMS provides specialized spatial analytical functions for characterizing remote sensing images, which

include fractal, wavelet, spatial autocorrelation, and other analytical functions (Lam et al., 2002). ICAMS can compute fractal dimension and spatial autocorrelation indices either in a global or local fashion using a moving window filter (Arumugam et al., 2003).

An executable function called MWFDTPM.exe (Moving Window using Fractal Dimension of the Triangular Prism Method) has been developed for use in the ICAMS (Caird, 2001). The function calculates fractal dimension at the local level using the triangular prism method.

The parameters needed when using the executable function are the number of steps to iterate the prism size over; the method to increase prism size; the number of rows and columns of fractal dimension to calculate; the increment between window edges for each fractal dimension calculation; the size of moving window; and the starting row and column.

ICAMS also contains a module for analyzing the spatial autocorrelation of images (Lam et al., 2002). Spatial autocorrelation is an assessment of the correlation of a variable in reference to spatial location of the variable. Spatial autocorrelation measures the level of interdependence between the variables, the nature and strength of the interdependence.

Moran's *I* statistic is one of the most common ways of measuring the degree of spatial autocorrelation in areal data (Rogerson, 2001). Moran's *I* is calculated as follows:

$$I(d) = \frac{n\sum_{i}^{n}\sum_{j}^{n} w_{ij} z_i z_j}{W\sum_{i}^{n} z_i^{\,2}} \qquad [12]$$

where :

w_{ij} = weight at distance d, so that

w_{ij} = 1, if point j is within distance d of point I, otherwise w_{ij} = 0

z's = deviations

W = the sum of all the weights where $i \neq j$

Moran's *I* varies from +1.0 for perfect positive autocorrelation (a clustered pattern) to -1.0 for perfect negative autocorrelation (a checkerboard pattern) (Lam et al., 2002).

CHAPTER IV

FOREST CLASSIFICATION

Overview

One of the main objectives of forest management program is to ensure that the forests are managed in an ecologically sustainable manner. This objective is based on the importance of the values or the benefits which are generated by forests. Forests provide us with tangible and intangible benefits. The tangible benefits or the benefits which can be valued economically, mainly come from timber harvesting, although other sources such as ecotourism also count. Ecotourism is defined as responsible travel to natural areas that conserves the environment and sustains the wellbeing of local people (The International Ecotourism Community, 2003). The intangible benefits of forests include assets that are equally important, even though it is difficult to place any monetary value on them. Some of the intangible benefits that forests provide are habitat for organisms, water preservation, erosion prevention, and contribution to the quality of life of local people. Sustainable forest management requires knowledge of forest structure, composition, and diversity, which can be acquired through forest inventory and classification.

Forest classification can be performed using two methods. The first one is the conventional method, which involves surveying for ground observation and enumeration, to collect information. The second method is classifying forests through the utilization of remotely sensed data. This method can be performed in several different ways, but most of the times it involves the use of spectral analysis on satellite or aircraft images in

classifying forest vegetation. The use of remotely sensed data in forest inventory is more effective in terms of the cost and the time needed as opposed to the conventional forest inventory. However, the conventional method usually yields more accurate results.

In forest classification, Anderson level I class delineates forest land from non-forest land, while level II class distinguishes deciduous forest land and evergreen (conifer) forest land. Anderson level III class concerns species groups of forest vegetation, for example Aspen (*Populus*) and Maples (*Acer*) (Hoffer, 1990), and level IV class is species specific, for example Sugar Maple (*Acer saccharinum*) and Red Maple (*Acer rubrum*).

Michigan Forests

Michigan forests are located in the northern or western Lake States region. Other areas that belong to this region are the forested areas of Minnesota and Wisconsin, which are situated among Lakes Superior, Michigan, and Huron (Mladenoff and Host, 1994). Michigan lies largely within the northern hardwood forest region of the eastern United States, with areas of the central hardwood region extending up into the southern part of the state, and with pines, aspen, and swamp coniferous of boreal forest, occupying large areas in the north past. Due to glacial action and changes created by nature and man, lines between these broad forest classes are frequently irregular, and within each are many different types, phases, and temporary conditions, overlapping and changing with local variations of climate, soil, and moisture (Smith, 2002).

Michigan forests cover about the half of the state, and they contain rich species diversity. The hardwood (broadleaf deciduous) forest types, which account for 72 percent of the total growing stock volume, include the species associations of maple-beech-birch, aspen-birch, oak-hickory, and elm-ash-soft maple. Principal softwood (coniferous) forest types include the species associations of red-white-jack pine, spruce-fir, and northern white cedar (Michigan Department of Natural Resources, 2003).

The abundant diversity of tree species, and the lack of strong elevational or other environmental gradients have made Michigan forests difficult to classify. This condition has challenged the spatial and spectral resolution of available sensors and classification methods to provide useful forest type differentiation (Mladenoff and Host, 1994; Crow, 1994; Roller and Visser, 1960; Hudson, 1987).

One of the largest hardwood tree genus or tree species group in Michigan is oak (*Quercus*). This genus has approximately 58 species in the United States and Canada alone. The oaks are of major economic importance for wood products, as a result of their strength, durability, and beauty. The oaks are also important for wildlife, recreation, and aesthetic values in both rural and urban forests (Rauscher, 2002). Due to the value of the oaks, it is essential to be able to distinguish them from other tree species during forest classification in a forest management program.

Spectral Analysis of Forests

Forests use solar energy in the photosynthesis process, using mostly the blue through red visible light (400-600 nm) portion of the electromagnetic spectrum. The rate of photosynthesis increases along with the increase of light intensity, until it reaches a

maximum (called saturation point), and after that, it decreases as light intensity increases. This photoinhibition can prohibit the growth of vegetation (MacDonald, 2003).

To perform photosynthesis, trees have adapted their internal and external structures, which has a direct impact on how leaves and canopies appear spectrally when they interact with electromagnetic energy (Jensen, 2000). The structure of different vegetation types affects the total amount and spectral distribution of radiant flux leaving a vegetated canopy. Some factors such as Leaf-Area-Index (LAI) and Leaf-Angle-Distribution (LAD) also influence the reflection of incident light toward the sensor system (Jensen, 2000).

The use of multispectral remotely sensed satellite images in forest classification has been of mixed value since they are useful in discriminating forested area from non forested area, and also in discriminating deciduous and conifer trees, but rather poor in identifying specific subcommunities or individual species of trees. Average accuracies for satellite based classifications of northern boreal and northeastern hardwood forests have varied considerably, ranging from 40 to 95 percent. However, in forest management practices, information containing species specific or species group data is generally required by private and public land management agencies (Bolstad and Lillesand, 1992).

Regrettably, the accuracy of the automated spectral classification at species group level is still relatively low, especially for hardwood species. The accuracies have not usually been considered adequate for many research or management purposes except for very general questions at large spatial scales (Mladenoff and Host, 1994). The main reason for the low accuracy is the similar spectral characteristics shown by different

hardwood species, which makes it hard to distinguish among species, especially the discrimination of oak dominated hardwood forests.

To display the spectral characteristic of a particular object at certain wavelengths, a spectral reflectance curve can be used. The curve shows how the reflectance value of the object varies when plotted against different wavelengths in the electromagnetic spectrum. Figure 11 shows the spectral reflectance characteristics of healthy green vegetation. A typical healthy green leaf absorbs radiant energy efficiently in the blue and red portions of the electromagnetic spectrum, and highly reflects energy in the near-infrared portions of the spectrum (700 – 1200 nm). There are a couple of reasons which cause healthy plant canopies to have such high near-infrared reflectance. First, a leaf in the canopy already reflects 40 – 60 percent of the incident near infrared energy from the spongy mesophyll, and second, the remaining 45 – 50 percent of the energy transmitted through the leaf is being reflected once again by leaves below it (Jensen, 2000).

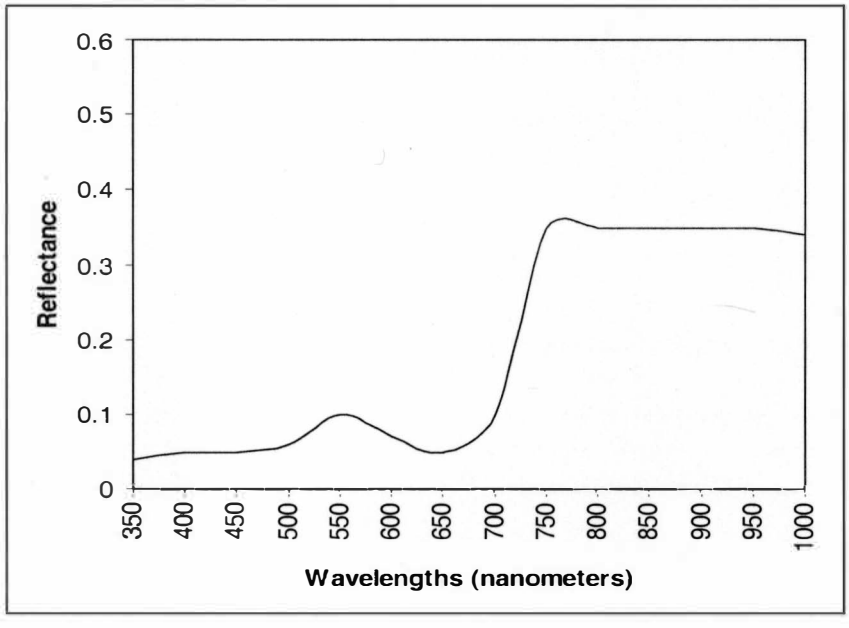

Figure 11. Spectral Reflectance Characteristics of Healthy Green Vegetation

The spectral reflectance curves for some hardwood species have a very high similarity among them. To accommodate the difficulty in discriminating hardwood species, some techniques have been incorporated in spectral analysis method, in order to achieve higher accuracy of the classified data.

Ancillary Information

One of the alternative techniques involves combining the images being classified with ancillary information such as soil type, elevation, and terrain position. Bolstad and Lillesand (1992) combined *a priori* information (soil and terrain position) and Landsat Thematic Mapper (TM) data in a maximum-likelihood classification of two forested areas in northern Wisconsin. For one of the areas, the classification accuracy reached 94 percent for northern hardwoods, red pine, jack pine, pine/hardwood, upland brush, lowland conifer, lowland brush, sphagnum, lowland vegetation, crop/pasture, soil/urban, aquatic vegetation, and water. The accuracy was 24 percent higher compared to the same area classified without the use of ancillary data. However, genus or species level discrimination was not obtained for most forest types.

Hierarchical Classification

Hierarchical classification uses prior classification in subsequent rounds in an attempt to increase the classification accuracy. High spatial resolution digital multispectral images have been used in classifying forest ecosystem near Barrier Lake in Kananaskis Country, southwestern Alberta, Canada (Gerylo et al., 1998). The images, which were taken in July, were classified using a maximum likelihood classification method applied in a hierarchical fashion. Initial accuracy was low, but the hierarchical

decision process increased average accuracy to over 65 percent for a limited selection of stand types. Species composition classification accuracy was higher for trembling aspen (*P.tremuloides*) (89 percent) than for lodgepole pine (*Pinus contorta*) (80 percent) and white spruce (*Picea glauca*) (84 percent).

Vegetation Indices

Vegetation indices are defined as dimensionless, radiometric measures that function as indicators of relative abundance and activity of green vegetation, often including leaf-area index (LAI), percentage green cover, chlorophyll content, green biomass, and absorbed photosynthetically active radiation (Jensen, 2000). Vegetation indices may be used to increase the degree of separation between land use type, especially discriminating forested areas and non forested areas, by bringing out small differences between various vegetation classes. Indices are used to create output images by combining the DN values of different bands (ERDAS, 2002). There are several vegetation indices, but the most commonly used is the Normalized Difference Vegetation Index (NDVI). This index is related to the proportion of photosynthetically absorbed radiation, and can be computed from the equations:

$$\text{NDVI} = \frac{\text{Infrared reflectance} - \text{Red Reflectance}}{\text{Infrared reflectance} + \text{Red reflectance}}$$

High index values are associated with vegetated areas due to their relatively high near infrared reflectance and low visible reflectance (Lillesand and Kiefer, 2000). Healthy green vegetation generally reflects 40 to 50 percent of the incident near infrared energy, with the chlorophyll in the plants absorbing approximately 80 percent to 90 percent of the incident energy in the visible spectrum. Reversibly, dead or senescent

vegetation reflects a greater amount of energy than healthy green vegetation throughout the visible spectrum, and reflect less than green vegetation in the reflective infrared region (Jensen, 1996). Rock and bare soil areas will have similar reflectance in the two bands, which results in near zero index value. Other features such as water, clouds, and snow will have negative index values due to their high visible reflectance values and low near infrared reflectance (Lillesand and Kiefer, 2000).

Phenological Information

Another technique to improve the accuracy of forest classification is the use of phenological information of vegetation or forest cover type. This technique requires analysis of imageries from various seasons of the year to separate a greater variety of forest cover type classes (Wolter et al., 1993; Mladenoff and Host, 1994). Timing is important when attempting to identify different vegetation types or to extract useful vegetation biophysical characteristics from remotely sensed data (Jensen, 2000). The accumulation or unmasking of pigments such as anthocyanins (responsible for scarlet to red leaf coloring), carotenoids (orange to yellow coloring), tannins (brown coloring), and xanthophylls (yellow coloring) following the denaturing of chlorophyll are responsible for spectral change (Boyer et al., 1988; Wolter et al., 1995). Changes in spectral reflectance caused by phenological differences among temperate forest tree species may allow for forest cover type classification at species group level on a regional scale (Wolter et al., 1995). An image from a leaf-on season (summer) would have different spectral and spatial characteristics from another image of the same area taken in a leaf-off season (winter), and this difference presents unique forest classification opportunities.

Several major tree species that are not distinguishable on peak summer imagery have characteristics that make them separable at other times of the year. These include differences such as early fall coloring of maples, late retention of oak leaves, early spring leaf-out of aspen, and detection of understory conifer layers during winter. Hence, a knowledge of the phenological characteristics of the vegetation within the area of interest has the potential to be a useful information in helping to choose the optimal time of year to collect the remotely sensed data to discriminate one vegetation type from another.

Schriever and Congalton (1993) used Landsat TM imagery covering three key dates to determine if phenological differences could improve forest classification accuracy of a forested area in southern New Hampshire. Separate classifications were performed on images from May (bud break), September (stable growing season), and October (senescence). They found that the October scene provided the best discrimination among the hardwood species American beech, (*Fagus grandifolia*), northern red oak (*Quercus rubra*), and red maple (*Acer rubrum*), with the classification accuracy of 74 percent.

Kalensky and Scherk (1975) tried to classify a forested area near Ottawa, Canada, using various combinations of spring to autumn Landsat Multispectral Scanner (MSS) data. They found that imagery from June, September, and October provided the best results over all other single and or multiple date classifications tested (84 percent of accuracy). They also concluded that the collective use of these scenes mitigated the effects of individual image noise.

Wilson (1997) investigated the use of winter (February) Landsat TM data in discriminating between deciduous tree species in Michigan's northern Lower Peninsula,

based on the assumption that the bark type and branch configuration might help in identifying stand density and composition. Images from summer season might not provide this information since the leaves on the trees dominate the spectral response of the stand. A summer dataset (September) of the same area was analyzed as well for the accuracy comparison. It was found that the winter data yields higher percentages for the less dense sugar maple (*Acer saccharum*), mixed deciduous and beech/birch categories.

The use of multi-temporal data in forest classification in the northern Lake States region was also utilized by Wolter et al. (1995). Landsat TM data from early summer was used in conjunction with four Landsat MSS dates to capture phenological changes of different tree species. The overall classification accuracy was 83.21 percent, and the forest classification accuracy was 80.1 percent. Among the 22 forest types classified, multi-temporal analysis helped in classifying 13 types. Species that were successfully classified include trembling aspen, sugar maple, northern red oak, northern pin oak (*Q. Palustris*), black ash (*Fraxinus nigra*), and tamarack (*Larix laricina*).

Texture Analysis in Forest Classification

In addition to using spectral analysis, texture analysis has also been used in forest classification attempts. Gordon and Philipson (1986) tried to separate fruit tree orchards from mixed deciduous forest using TM data in New York State. A binary image was produced after the original image had been through a texture enhancement, band (3 and 4) ratioing, and a smooth filtering. The binary image was included in a supervised maximum likelihood classification of six bands of single date TM imagery, and the result

was a reduction in misclassification of deciduous forest as fruit tree orchards from 75 percent to approximately 7 percent.

Moskal and Franklin (2001) have reported an improvement of classification accuracies of the Kananaskis Barrier Lake mix wood forest in the Rocky Mountain region of Alberta, Canada with the use of texture channels, using data taken by the Compact Airborne Spectrographic Imager (*casi*) with three different resolutions (60 cm, 1 m, and 2 m). Seven spectral bands, and five textural bands derived from second-order texture measures of the brightness component of the imagery were used in discriminant analysis to determine the usefulness of the textural information. These bands were also used to compare two sample stratification schemes (six classes and thirteen classes). On average, they found that the use of texture channels improved the per plot classification accuracies by 17 percent compared to using the spectral bands alone. The classification with thirteen classes outperformed the six classes scheme by 14 percent, with results of 87 percent of accuracy and a KHAT of 0.85 compared to the 72 percent of accuracy and KHAT of 0.73 of the six classes scheme. They also found that the best classification results were achieved with the use of the highest image resolution of 60 cm.

Jakubauskas (1997) conducted a study to determine if significant differences in texture occurred among six successional stages of lodgepole pine (*P. contorta*) (Postfire regeneration, Dense and small diameter lodgepole pine, Mature lodgepole pine forest, Mesic sites: mixed pine/fir overstory, Xeric sites: lodgepole pine overstory, and Affected by pine-bark beetle) within the Central Plateau of Yellowstone National Park, Wyoming. A first order statistical measure of texture was computed for each of the six reflective Landsat TM bands, three Tasseled Cap components, and a NDVI. Texture values were

found high for early successional sites (post-fire), decrease in mid-succession, and increase as stands progress to uneven aged, uneven-height old growth.

A similar type of study was performed by Moskal and Jakubauskas (2001). They conducted a discrimination of the lodgepole pine forest development stages in the same area. This time, they used Landsat ETM+ data, and utilized a 2nd order image texture derivative (entropy). The texture measure was based on the 15 m per pixel resolution of Landsat ETM+ panchromatic band. The image texture was combined with the NDVI image of the area, and resulted in about 30 percent improvement of classification accuracy with overall classification results of over 90 percent. The most significant improvement (36 percent) is for the uneven age, uneven canopy, Engelmann spruce (*Picea engelmanni*) and subalpine fir (*Abies lasiocarpa*) stands, which has proven to be a difficult age class to map. For the seedling and 100 year-old pine stands, the texture addition improved the accuracy by 12 percent.

CHAPTER V

METHODOLOGY

Study Area

The study area chosen for this research is the area of Fort Custer Training Center (FCTC) (Figure 12). The FCTC is located in Calhoun and Kalamazoo counties, in the southwestern part of the lower peninsula of Michigan. The size of the area is 7,570 acres, with more than 75 % of the area covered in forests. The FCTC is bounded by Interstate 94 to the south, and by Fort Custer Recreation Area and Kalamazoo River to the north. The city of Battle Creek is located 2 miles northeast of the area.

The FCTC provides a large tract of relatively unfragmented deciduous forest which is rare in this region of the state and the country. Table 2 shows the common species found in the area. The oaks are the most dominant forest type in the area, although other species of hardwoods and softwoods are also found at the site.

Table 2. Common Species at the Fort Custer Training Center

Common Name	Latin Name	Hardwoods/Softwoods
Northern red oak	*Quercus rubra*	Hardwoods
Black oak	*Q. velutina*	Hardwoods
Scarlet oak	*Q. coccinea*	Hardwoods
Bigtooth aspen	*Populus grandidentata*	Hardwoods
Black cherry	*Prunus serotina*	Hardwoods
Black locust	*Robinia pseudoacacia*	Hardwoods
Black walnut	*Juglans nigra*	Hardwoods
Red maple	*Acer rubrum*	Hardwoods
Red pine	*Pinus resinosa*	Softwoods
White pine	*P. strobes*	Softwoods

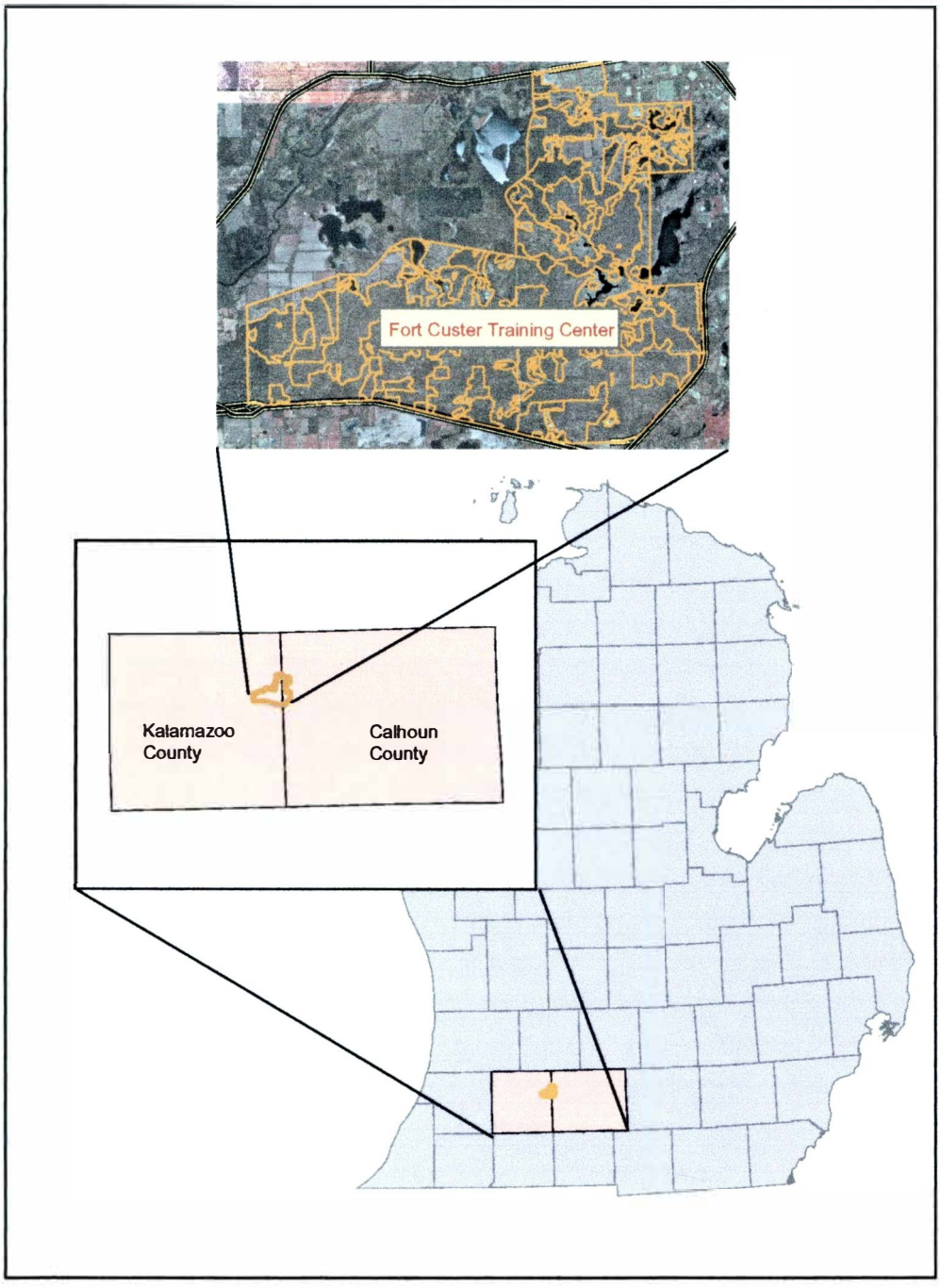

Figure 12. Study Area: The Fort Custer Training Center, Michigan

Data

Landsat ETM+ panchromatic and multispectral imagery from two different dates were made available for the research. The bands used in the study were band 1, 2, 3, 4, 5, 6, and 8. Table 3 shows the spectral range for each band in the electromagnetic spectrum.

Table 3. Landsat ETM+ Bands Used in the Study

Band	Wavelength (μm)
1	0.45 - 0.51
2	0.52 - 0.61
3	0.63 - 0.69
4	0.75 - 0.90
5	1.55 - 1.75
6	10.40 - 12.5
8	0.52 - 0.90

The resolution for ETM band 1 – 6 is 30 m, while the panchromatic band (band 8) has a 15 m resolution. The dataset were acquired on June 6 and October 28, 2000 along path 021 and row 31. A subset that covers the study area was made for each full Landsat scene. Figures 13 and 14 show the false-color composite (ETM+ band 4, 3, 2 = R, G, B) of the study area from both dates. The use of Landsat data from different dates was meant to catch the phenological condition of vegetation, particularly hardwoods. The June scene represented trees at early stage in the growing season by capturing hardwood leaf flush, while the October scene captured peak senescence for most hardwoods, especially for oak trees. The oak species in the Lake States region tend to hold their leaves longer than the other hardwood species in autumn (Wolter et al, 1995). The late October ETM+ scene was used to give oak species a distinct spectral reflectance

compared to reflectance of other hardwood species that may have been in the leaf-out stage. Separate classifications were performed on each scene to compare the results.

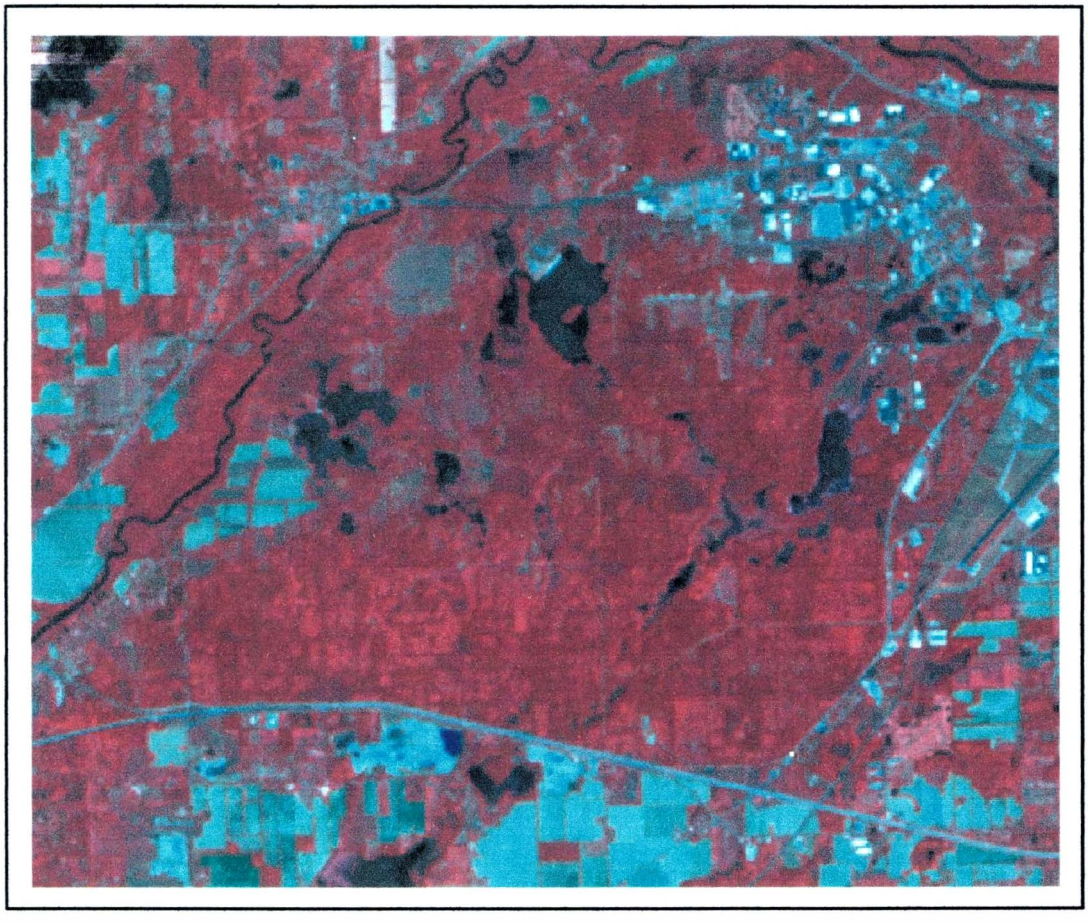

Figure 13. Landsat Image of FCTC on June 6, 2000

The data that served as a reference for the research is a polygon shapefile of forest cover type of the study area made available by Fort Custer Training Center (Figure 15). The forest cover type map was the result of the 1999 forest inventory of FCTC, completed by Ogden Environmental and Energy Services Company, Inc. The shapefile was then converted into a geodatabase, for an easier editing session.

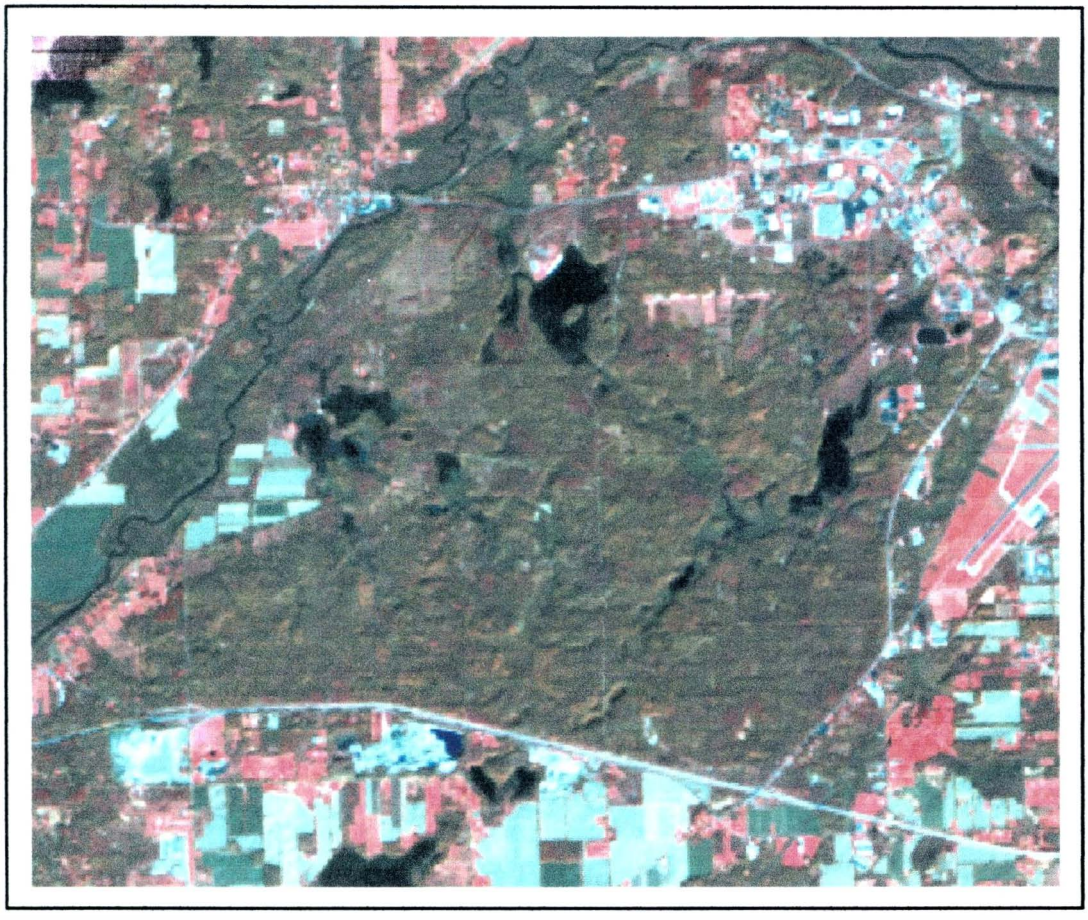

Figure 14. Landsat Image of FCTC on October 28, 2000

Another dataset used in the research was an orthophoto of the study area, provided by the GIS Research Center at Western Michigan University. The photo was obtained on April 13, 1999, and has a spatial resolution of 1 meter. The high resolution orthophoto assisted in visual analysis of the ETM+ scene, and was also used to verify the forest cover type map. Figure 16 shows the orthophoto of the area. All datasets were geometrically registered in zone 16N of the UTM coordinate system and WGS 1984 datum.

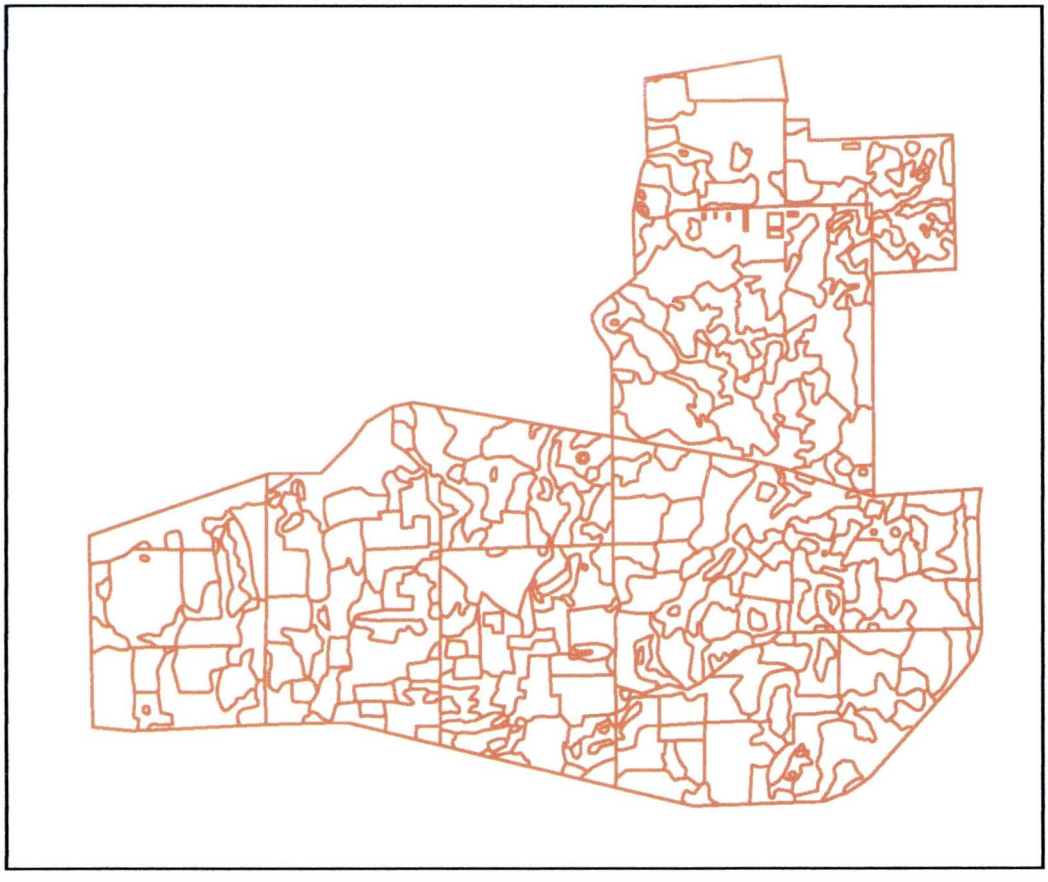

Figure 15. The Original Forest Cover Type Map

Methods

The original forest cover type map came with 22 different classes. The high number of classes, despite providing more details to the map, is not favored in this particular study, not only because it would result in a highly complex accuracy assessment, but also for the fact that the classes do not match with the objective of the research, which is to distinguish oak species from other hardwood species.

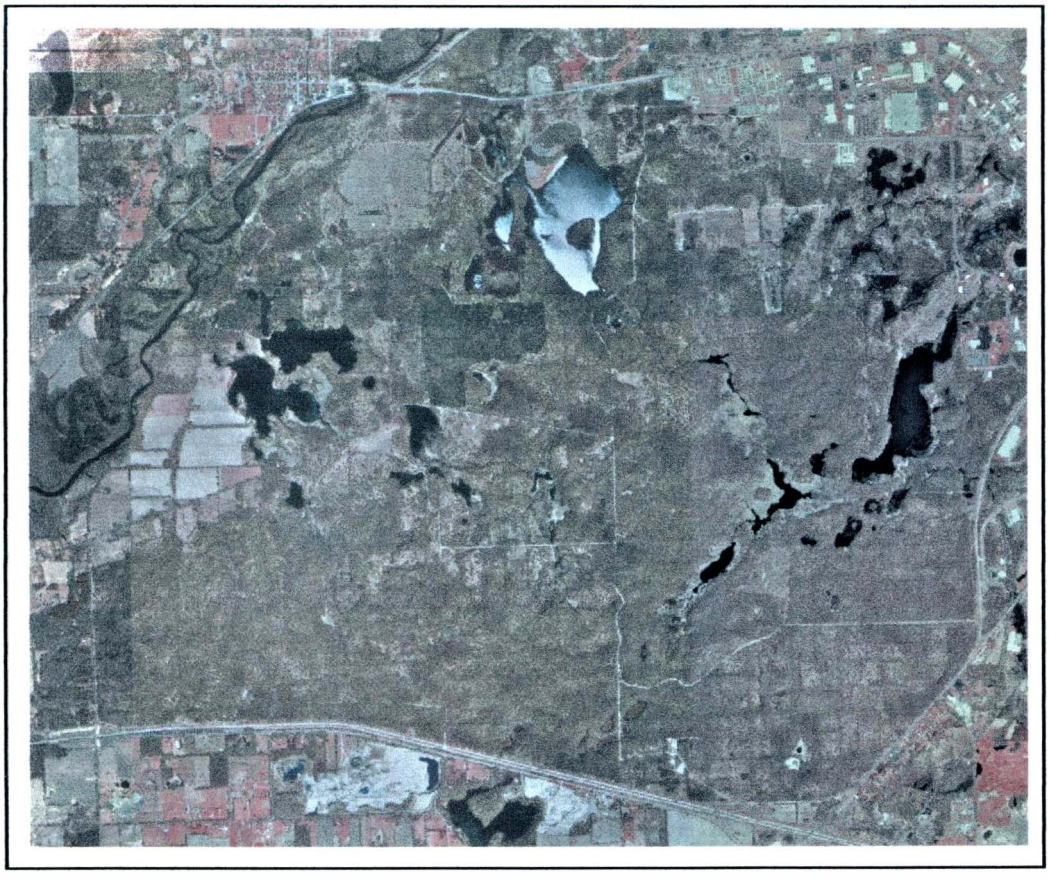

Figure 16. The Orthophoto of FCTC

For the reason above, a simpler classification scheme was established. The new classification scheme has eight classes that represents more general or broader categories of the area. Table 4 displays the new classification scheme with its eight classes.

Urban category includes areas with little or no vegetation that have been disturbed by human activity other than for the production of agricultural crops. Examples in the study area include areas with buildings and roads. Conifer category

includes all needle-leafed tree species with a pyramidal or cone-shaped canopy, or life form. Trees in this class are Jack Pine, White Pine, and Red Pine

Table 4. Classification Scheme

Class	Class Name
1	Urban
2	Conifer
3	Pure Oaks
4	Other Hardwoods
5	Mixed Oak-Hardwoods
6	Shrubs/Brush
7	Open Dry Land/Grassland
8	Water

Pure Oaks category includes areas where 75 percent of the vegetation cover types are mixed species of oaks. Other Hardwoods category comprises areas with mixed hardwood species, where the oak species are less than 25 percent. Meanwhile, Mixed-Oak Hardwoods category covers areas where about 50 percent of the vegetation cover types are oak species, and 50 other percent are hardwood species other than oak.

Shrubs/Brush category comprises areas dominated by shrubs generally greater than 0.5 m in height with individuals and clumps not touching to interlocking. Shrub canopy cover is generally greater than 25 percent while tree covers are less than 25 percent. Open Dry Land/Grassland covers areas no or little low vegetation, usually less than 0.5 meter in height. Water category includes areas where water is equal or greater than 70 percent. Also included in this class are wetlands.

The geodatabase of the forest cover type map was then overlaid with the orthophoto. From a visual perspective, a few of the polygon boundaries do not align perfectly with what is most likely to be a class boundary in the orthophoto. Hence, an editing session to adjust the boundary of the polygons was performed. This operation was done using ArcGIS 8.3 (Environmental System Research Institute, 2002).

Next, in the attribute table of the map, each polygon in the map was given a code (1 to 8) that reflects the class to which it belongs in the new classification scheme. A dissolve operation was performed based on the new code created, so that areas with the same code that are sharing boundaries are aggregated. This way, a new forest cover type map with 8 classes was created (Figure 17). This operation reduced the number of polygons in the map, from 360 in the original map to 160 in the new map.

NDVI images were derived from both multispectral ETM+ scenes to help in the classification process. On the NDVI images and the panchromatic images for both the ETM+ June and October scenes, local fractal dimension and Moran's *I* measurements were performed using the MWFDTPM program. Measurements on the Landsat ETM+ panchromatic image, which has a 15 meter resolution, was performed with a two pixels increment between measurements. The resulting 30 meter resolution images match the multispectral images and the NDVI images derived from them.

Moving windows with the size of 9 x 9, 11 x 11, 13 x 13, 15 x 15, 17 x 17, 19 x 19, and 21 x 21 were used to see if there is a significant difference in the results

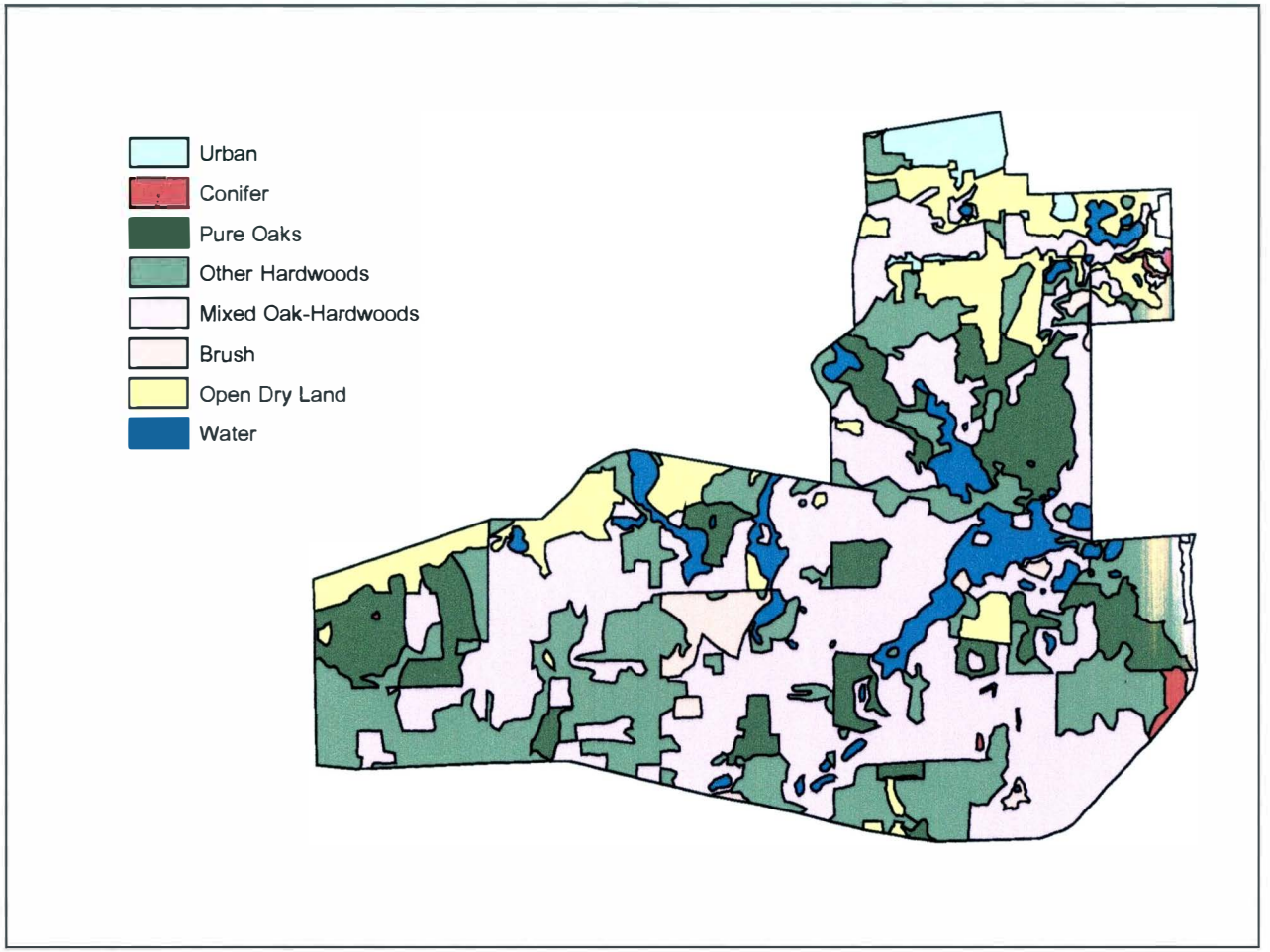

Figure 17. Forest Cover Type Map

between different sizes of windows. Texture measurement is influenced by the size of moving window used. Small window sizes would result in less number of points in the regression line, making the regression less stable, and can yield a noisy image (Emerson, 2003), while large window sizes lose some texture details.

The output of the MWFDTPM program was in the form of text files that needed to be converted to Arc/Info grids. The conversion was performed using ArcToolbox. The projection of the grids was then defined to match the existing images to be used in the classification process. The grids were subsequently imported and rescaled to unsigned 8 bit integers with .img extension, to be run in ERDAS 8.6 (Leica Geosystem, 2002).

To include the fractal dimension and Moran's *I* measurement into the classification, the resulted images were added as supplemental layers for the classification process. To do so, they were put together with multispectral bands (band 1-6) of the ETM+ scenes in layer stacks.

The next step was to build training areas for supervised classification on the scene. After that, the training sites were evaluated by looking at their histograms using the signature editor in ERDAS. Histograms for each training site were checked to help in determining if the training sites were good enough to represent the scene. A refinement process for the training sites was done accordingly, which included deleting, adding, and merging them.

With these training sites, supervised classifications were performed on both the June and October scenes using the maximum likelihood classifier. For each

window size on each scene, 7 different designs of classifications were applied. These designs utilized different combination of bands for the classification process. The 7 designs of classifications are listed as follows:

Table 5. Classification Designs

Design	Band Combination
1	Multispectral bands only (6 bands)
2	Multispectral bands + fractal dimension of panchromatic image
3	Multispectral bands + Moran's *I* measurement of panchromatic image
4	Multispectral bands + fractal dimension of NDVI
5	Multispectral bands + Moran's *I* measurement of NDVI
6	Multispectral bands + fractal dimension of panchromatic image + fractal dimension of NDVI
7	Multispectral bands + Moran's *I* measurement of panchromatic image + Moran's *I* measurement of NDVI

To validate the classification results, accuracy assessments were performed. In the assessment process, the classified categories were compared to the categories in the forest cover type map (the true categories). The center points of each polygon were used as the sample points for the classification accuracy assessment. One reason for using the center points is that the boundaries of the forest cover polygons are fuzzy boundaries, meaning that there is no clear distinction or fixed boundaries when moving from one cover type to another. The center of a polygon tends to be more homogenous in species group or species association identification and tends to be less homogenous in outward direction, approaching the boundary of the polygon.

For instance, the pixel at the center of a pure oak polygon will more likely have a better chance to be actually representing an oak tree than any other pixel elsewhere in the polygon, especially pixels along the boundary, where other species of trees may be occupying the place. The use of the center point of polygons as the sample points also reduced the chance of error caused by misregistration between images. For a couple of polygons whose size is less than 1000 acres, the center points were not used, which made a total number of sample points used to be 160.

The center point of each polygon was located in the map using Centroidlabel command in ArcMap, and these points were ensured to be inside the polygons (Figure 18). The x and y coordinates of these points were generated, and both true and classified class was determined for each point. The classified data were assessed to determine their accuracy, and contingency tables were produced to summarize the accuracy assessment for each classification. The results for these accuracy assessments were compared to see if there is any significant difference between them.

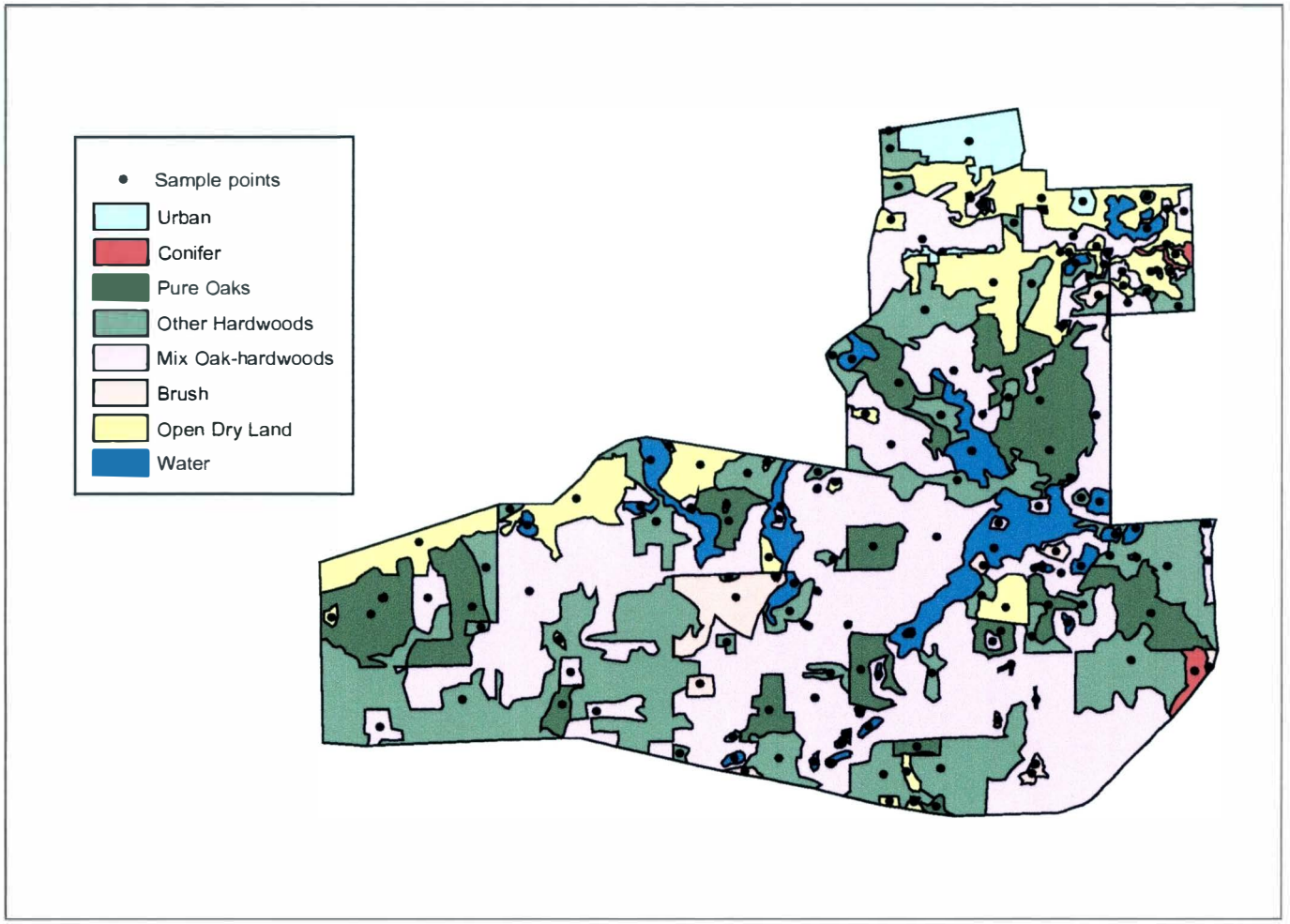

Figure 18. Sample Points for Accuracy Assessments

CHAPTER VI

RESULTS AND DISCUSSION

Multispectral Classification

In general, the classification results for both the June and October scenes are relatively low in accuracy. The overall accuracy for multispectral classification of the June Scene (Figure 19) was 30.25 percent, with Cohen's Kappa value of 0.2012 (Table 6). Meanwhile the overall accuracy for multispectral classification of the October scene (Figure 20) was 43.21 percent, with Cohen's Kappa value of 0.3229 (Table 7). The lower result for the June scene was anticipated, because on the summer scene, the all green tree species do not have easily distinguishable spectral characteristics. Some individual producer's accuracies were higher when computed using the summer scene, however the user's accuracies for the particular categories did not increase as well.

Due to the variability of trees' spectral reflectance, the accuracies for overall and individual categories of the fall scene were higher for every category except for open dry land, which had a better accuracy in the June scene. Although higher than the accuracy for the June scene, the 43.21 percent classification accuracy of the October scene was still very poor. A great amount of confusion occurred for tree stands categories. Pure oak stands were often classified as other hardwoods or mixed oak-hardwoods stands, and vice versa. This may have been due to the acquisition

time of the imagery (October 28, 2000), in relation to vegetation phenology and environment factors influencing it.

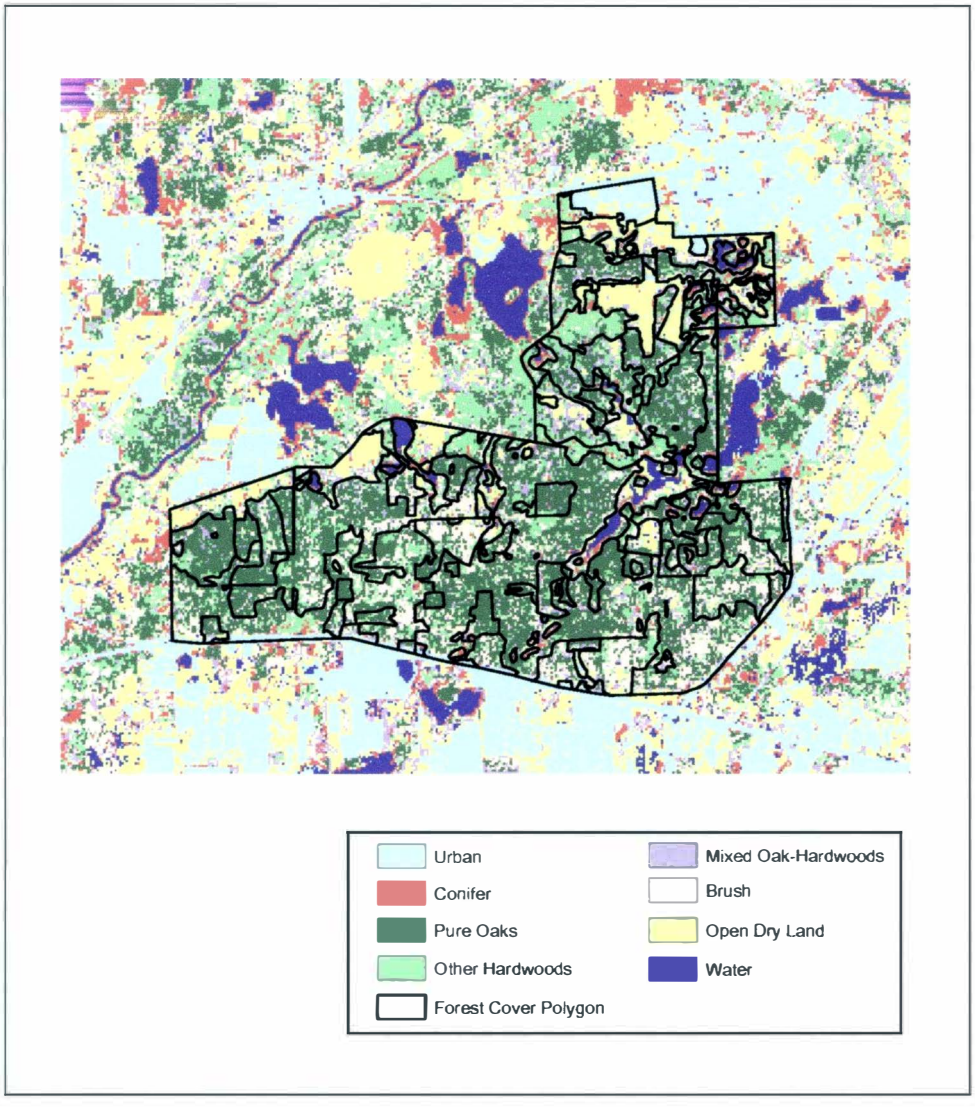

Figure 19. Classified ETM+ June Scene Using Multispectral Bands Only

The record from the timeseries archive of the National Climatic Data Center indicated that the average temperatures and precipitation for Michigan and all other states in the Midwest region were above normal in October 2000 (National Climatic

Table 6. Classification Accuracy of the June Scene Using Multispectral Bands Only

	Reference Data										
Class.Data	Urban	Con	Oaks	Others	Mix	Brush	ODL	Water	Tot	User's acc	Kappa
Urban	2	0	0	1	0	2	2	0	7	28.57%	0.2676
Con	0	2	0	3	0	1	0	7	13	15.38%	0.1213
Oaks	0	3	12	17	16	2	1	9	60	20.00%	0.1123
Mix	0	0	1	11	5	1	4	7	29	37.93%	0.155
OH	0	0	1	1	1	0	2	0	5	20.00%	0.04
Brush	1	1	1	9	2	2	1	4	21	9.52%	0.0482
ODL	1	0	1	1	2	0	11	2	18	61.11%	0.5532
Water	0	0	0	0	1	0	0	8	9	88.89%	0.856
Totals	4	6	16	43	27	8	21	37	162		
Prod.acc	50.00%	33.33%	75.00%	25.58%	3.70%	25.00%	52.38%	21.62%			

PCC	Kappa
30.25%	0.201

Data Center, 2003). This warm month may have delayed senescence of tree species in the area. Despite the intention of picking up the peak senescence of the oak trees by using the October scene, the senescence of oak species might not have progressed far enough on that particular date, which left trees from different species to still having the same green color of leaves. This poor discrimination between tree stands was another confirmation to the difficulty of distinguishing among northern hardwood species, especially oak species, because of their very similar spectral characteristics.

Another possible reason for this low accuracy was the varied condition of tree stands or polygons that were not specified in the reference data. For example, in a white pine stand, there were some scattered red oaks, which made the pine stand was actually not pure. Same thing happened to some pure oak stands, where heavy black cherry regeneration took place. This should have made the oak stands fall into mixed oak-hardwoods category, but instead they were still called oak stands. Variation on

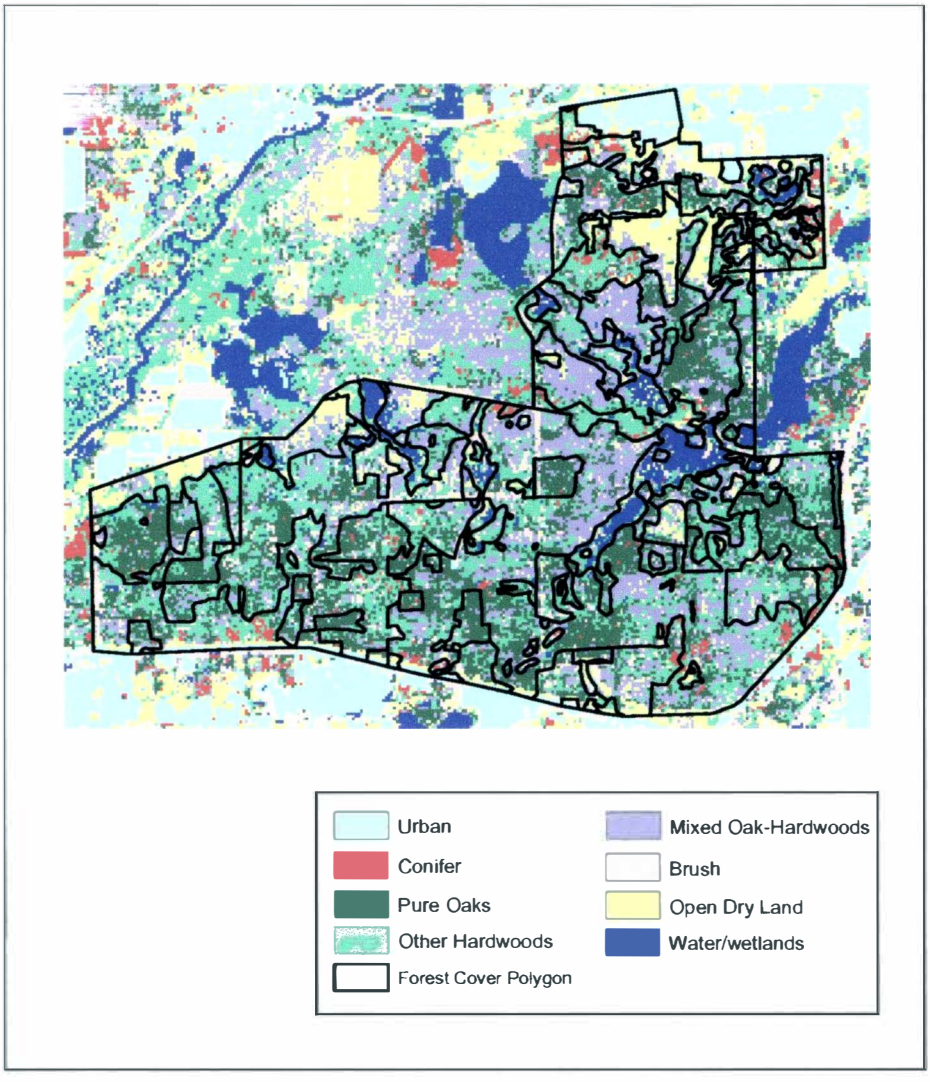

Figure 20. Classified ETM+ October Scene Using Multispectral Bands Only

canopy closure and forest floor condition may also have affected the spectral reflectance of the trees. For instance, a tree stand or a polygon can have an open forest floor with sparse understory vegetation, where another stand from the same category possesses heavy or dense understory vegetation. This variation would cause differences in their spectral reflectance.

Table 7. Classification Accuracy of the October Scene Using Multispectral Bands Only

	Reference Data										
Class.Data	Urban	Con	Oaks	Others	OH	Brush	ODL	Water	Tot	User's acc	Kappa
Urban	2	0	0	0	0	1	0	0	3	66.67%	0.6582
Con	0	4	0	2	1	0	1	1	9	44.44%	0.4231
Oaks	0	1	8	11	7	3	0	5	35	22.86%	0.144
Other	0	1	6	20	3	0	5	7	42	47.62%	0.2869
Mix	1	0	2	5	15	1	5	5	34	44.12%	0.3294
Brush	0	0	0	1	1	1	1	6	10	10.00%	0.0532
ODL	1	0	0	3	0	2	9	2	17	52.94%	0.4593
Water	0	0	0	1	0	0	0	11	12	91.67%	0.892
Totals	4	6	16	43	27	8	21	37	162		
Prod.acc	50.00%	66.67%	50.00%	46.51%	55.56%	12.50%	42.86%	29.73%			
	PCC	Kappa									
	43.21%	0.3229									

The greatest amount of confusion occurred for the brush category for both scenes. In many instances, the pixels in lowland brush areas were classified as water, while pixels in upland brush areas were classified as hardwoods stands.

The urban category had the same producer's accuracy for both scenes (50 percent), however, when using the June scene, some urban pixels were misclassified as tree stands, brush or open dry land, which meant the user's accuracy for the urban category was better when using the October scene (66.67 percent). This may have been because some anthropogenic materials that characterize urban land cover such as roads and buildings are covered with tree canopies during the summer, when the trees are at their highest level of leaf production.

Water had a low producer's accuracy but the highest user's accuracy from all the categories in both scenes, and the use of the October scene slightly gave a higher result (91.67 percent) than the use of the June scene (88.89 percent). The omission errors for this category often came from classifying pixels in water category as

hardwood stands. The reason for this misclassification might have been the fact that some of the water bodies have black willow species growing on their banks, and their canopy may cover some part of the water body, allowing the pixel to be classified as hardwood stands. Meanwhile, conifer was better classified using the October scene (producer's accuracy 66.67 percent and user's accuracy 44.44 percent). This again, may have been caused by the similarity in spectral reflectance of different tree species during the growing season.

Local spatial measures (fractal dimension and Moran's *I*) were obtained from both scenes using different classification designs. Figure 21 shows fractal dimension and Moran's *I* measures computed from the October scene using one of the classification designs. Based on the figure, the contrast between land and water is obvious, however, it is still hard to recognize forest cover type pattern visually. From the literature, it has been reported that texture measures can yield more accurate results if used together with traditional multispectral techniques. Hence, the results of texture measures were combined with the multispectral bands from both scenes, acting as additional layers in the classifications.

Multispectral Bands + Fractal Dimension Measures

Fractal Dimension Measures on Panchromatic Images

For both the June and October scenes, the addition of the local fractal dimension measures slightly improved the accuracy of the classification. Overall, the

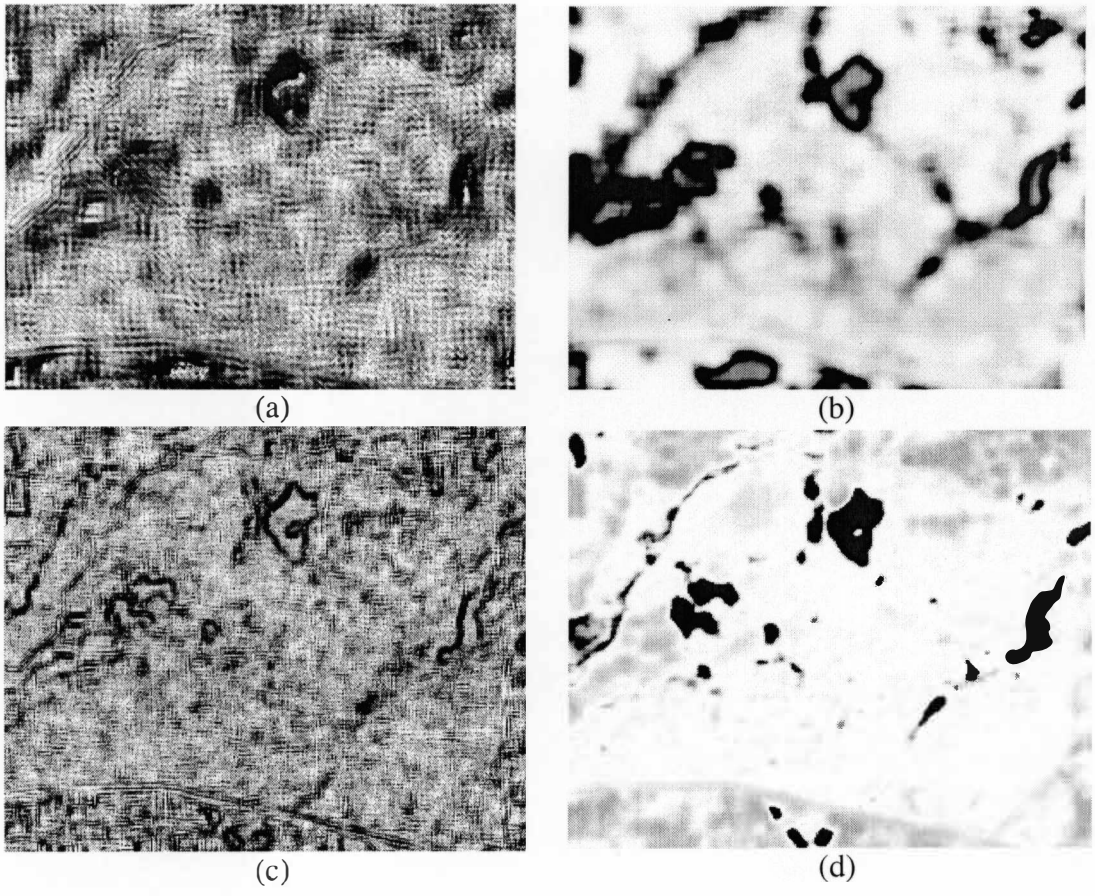

Legend. (a) Local Fractal Dimension of NDVI image
(b) Moran's *I* of NDVI image
(c) Local Fractal Dimension of panchromatic image
(d) Moran's *I* of panchromatic image

Figure 21. Local Spatial Measures on the ETM+ October Scene in an 11 x 11 Window

classification results for the June scene are less accurate than the results for the October scene. The accuracy for the multispectral classification of the June scene was only 30.25 % (Table 6). However, the fractal dimension measures seemed to work better on the June scene, since it gave a higher percentage of improvement. This may have been caused by trees' steeper leaf angle during the summer season.

Leaf orientation influences the amount of light absorbed by altering both the level of reflectance and the available cross-sectional area. In summer, the longer day light hours and the higher solar intensity received can be factors that cause vegetation photoinhibition. Steep leaf angles, caused by the upward movement of the leaf, decreases light capture when the sun is at high angles (midday or summer) to avoid photoinhibition, and to increase water use efficiency (Falster and Westoby, 2003). When looked at from above, trees with steep leaf angle may produce a more 'rough' texture compared to 'smooth' texture produced by trees with low/horizontal leaf angle.

The addition of fractal dimension measurement on the panchromatic image (design 2 classification) of the June scene improved the classification accuracy using all window sizes (Figure 22). Pure oak category had an improved user's accuracy for all window sizes using this design. The producer's accuracy of this category was either increased or remained the same compared to using multispectral bands alone (user's accuracy of 20 % and producer's accuracy of 75 %, Cohen's Kappa = 0.112). The highest improvement was achieved by the 15 x 15 window with 93.75 % producer's accuracy and 24.59% user's accuracy, with Cohen's Kappa value of 0.163.

The per-category improvement was also noticed for the Other Hardwoods category in response to the addition of fractal dimension measure of the panchromatic image in the classification, where the user's and producer's accuracy increased with the use of all window sizes. The highest improvement for user's accuracy was

observed with the use of the 15 x 15 window (56.52 %), with producer's accuracy of 30.23 % and Cohen's Kappa value of 0.4081.

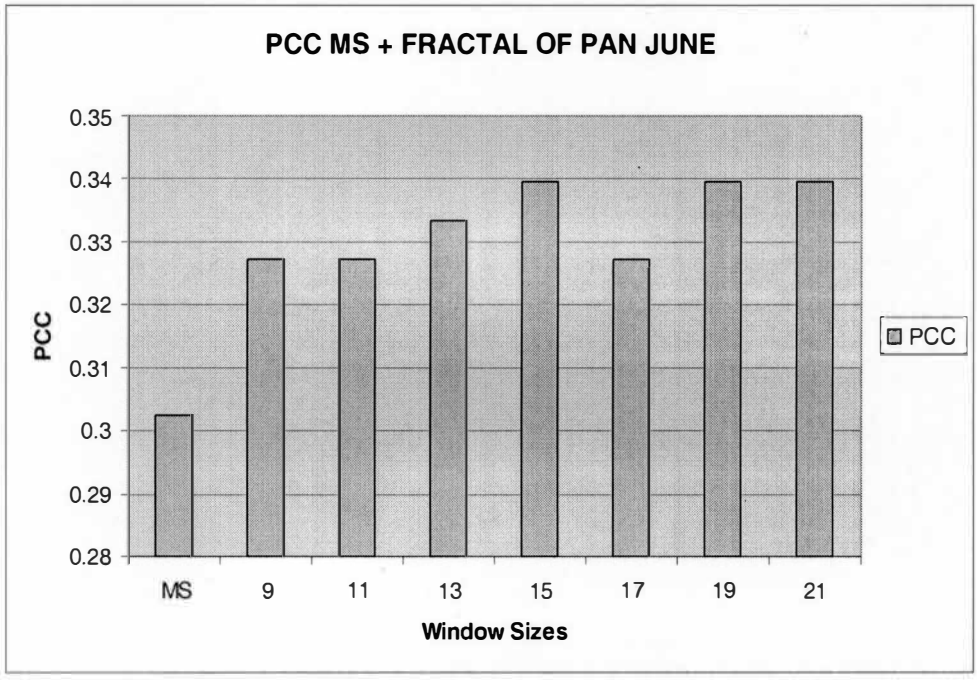

Figure 22. Percent Correctly Classified of the June Scene Using Design 2 Classification with Different Window Sizes

Water category accuracy did not seem to be affected by the use of fractal dimension measures on the June panchromatic scene. Meanwhile, the user's accuracy for brush category increased for all window sizes, although the producer's accuracy did not always follow the same pattern (it either increased or remained the same).

Figure 23 shows that the local fractal dimension measurement on the October panchromatic image slightly improved the overall accuracy if used in a 9x9 (43.88 percent, Cohen's Kappa = 0.3277), an 11x11 (44.44 percent, Cohen's Kappa = 0.3295), and a 19x19 (45.06 percent, Cohen's Kappa = 0.3419) windows.

Meanwhile, larger window sizes (15x15, 17 x 17, and 21 x 21), with an exception of the 19 x 19 window, lowered the classification accuracy.

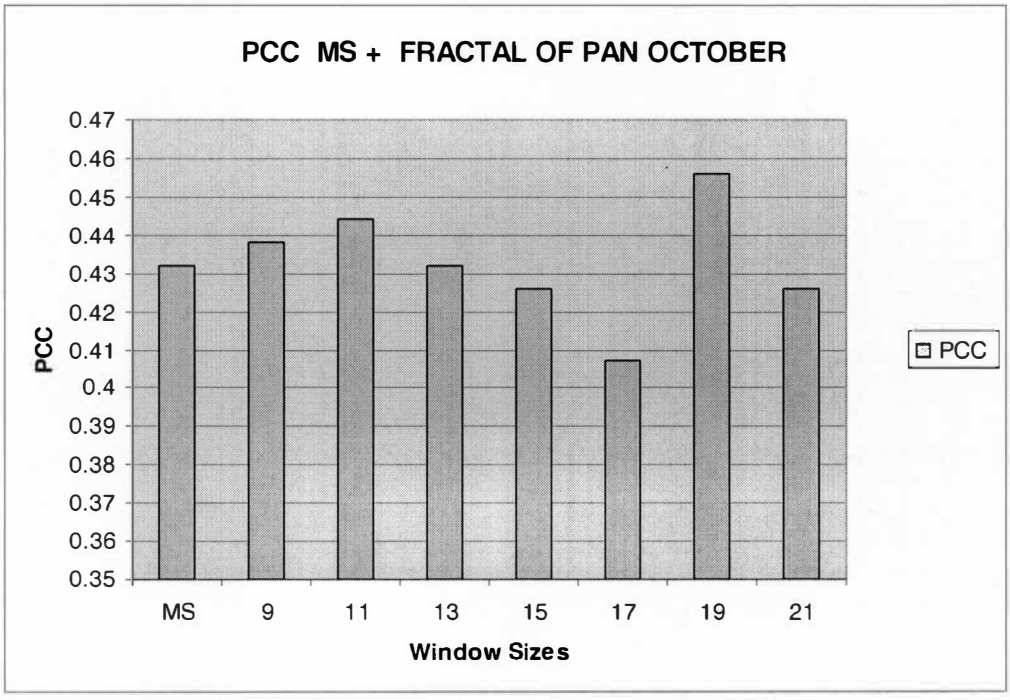

Figure 23. Percent Correctly Classified of the October Scene Using Design 2 Classification with Different Window Sizes

Nonetheless, the classification design using fractal dimension measure in the 13 x 13, 15x15, 17 x 17, and 21 x 21 windows caused increases in per-category accuracies for several categories. This was also true for the use of the 19x19 window. Conifer was one of the categories whose accuracies increased with this design type, when used in the 17 x 17 and the 19 x 19 windows. The improvement was about 12.7 percent for the 17 x 17 window, where the user's accuracy increased to 57.14 percent from 44.44 percent, and the Cohen's Kappa value increased to ●.554 from ●.423. For the 19 x 19 window, the improvement was 22.23 percent (user's accuracy

66.6 7 percent and Cohen's Kappa value of 0.653) compared to using the multispectral bands alone.

Again, the use of fractal dimension measure computed from the panchromatic image did not increase the accuracy of the water category. Meanwhile, the accuracy for pure oaks category improved with the use of the 11x11 window and the 19 x 19 window. The 11 x 11 window improved the user's accuracy by 7.44 percent and the producer's accuracy by 12.50 percent. The use of multispectral bands alone gave a user's accuracy of 22.86 percent and a producer's accuracy of 50 percent for pure oaks category, while the addition of fractal dimension measure increased the user's accuracy to 30.30 percent and the producer's accuracy to 62.50 percent. Meanwhile, the Cohen's Kappa value also improved from 0.144 to 0.227. With the 19x19 window, the user's accuracy improved to 28.13 percent and the producer's accuracy increased to 56.25 percent (Cohen's Kappa value of 0.203).

The highest overall accuracy for the October scene was achieved from the combination of multispectral bands and local fractal dimension computed of the panchromatic image (design 2 classification) using the 19 x 19 window (Figure 24), with the overall accuracy of 45.06 percent, showing a slight improvement of 1.85 percent (Table 8). The Cohen's Kappa value for this classification was 0.3419.

Fractal Dimension Measures on NDVI Images

For performance on NDVI images (design 4 classification), the local fractal dimension computed from the June scene increased the accuracy of classification

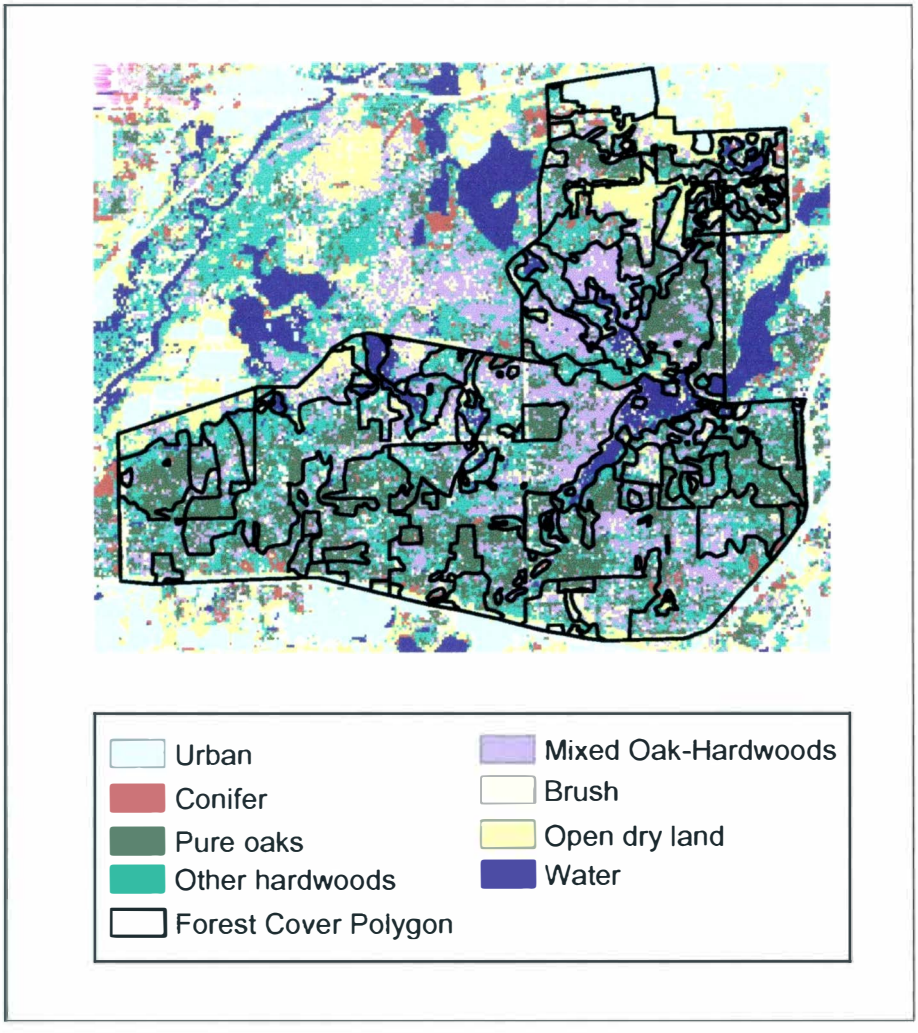

Figure 24. Classified ETM+ October Scene Using Design 2 Classification in a 19 x 19 Window

with the use of all window sizes except the 17x17 (Figure 25). To the contrary, the addition of fractal dimension measurement on October NDVI images did not change the accuracy of the classification, which was true for all window sizes.

Table 8. Classification Accuracy of the October Scene Using Design 2 Classification in a 19x19 Window

	Reference Data										
Class.Data	**Urban**	**Con**	**Oaks**	**Others**	**OH**	**Brush**	**ODL**	**Water**	**Tot**	**User's acc**	**Kappa**
Urban	2	0	0	0	0	1	0	0	3	66.67%	0.6582
Con	0	4	0	1	1	0	0	1	7	57.14%	0.5549
Oaks	0	2	9	8	6	2	0	5	32	28.13%	0.2025
Others	0	0	6	24	6	1	5	5	47	51.06%	0.3338
OH	1	0	1	4	14	1	5	6	32	43.75%	0.325
Brush	0	0	0	2	0	1	3	7	13	7.69%	0.029
ODL	1	0	0	3	0	2	8	2	16	50.00%	0.4255
Water	0	0	0	1	0	0	0	11	12	91.67%	0.892
Total	4	6	16	43	27	8	21	37	162		
Prod.acc	50.00%	66.67%	56.25%	55.81%	51.85%	12.50%	38.10%	29.73%			
	PCC	**Kappa**									
	45.06%	**0.3419**									

The use of NDVI images seemed to work better if combined with the panchromatic image. The addition of fractal dimension measurement on June NDVI images and panchromatic images together (design 6) increased the overall accuracy. For the June scene, this was true for all window sizes (Figure 26). This classification design performed in a 15x15 window produced the highest classification accuracy of all the June scene's classification (36.42 %), showing an improvement of 6.17 % compared with using the spectral bands alone (Figure 27). The Cohen's Kappa value for this classification was 0.2639 (Table 9).

The addition of fractal dimension measurement on the October NDVI and the panchromatic image together resulted in an improvement of the overall classification accuracy by 1.23 percent. This was true for the 15 x 15 window size, with the overall accuracy of 44.44 percent and Cohen's Kappa value of 0.3326 (Table 10). Meanwhile, for other window sizes, the addition reduced the classification accuracy.

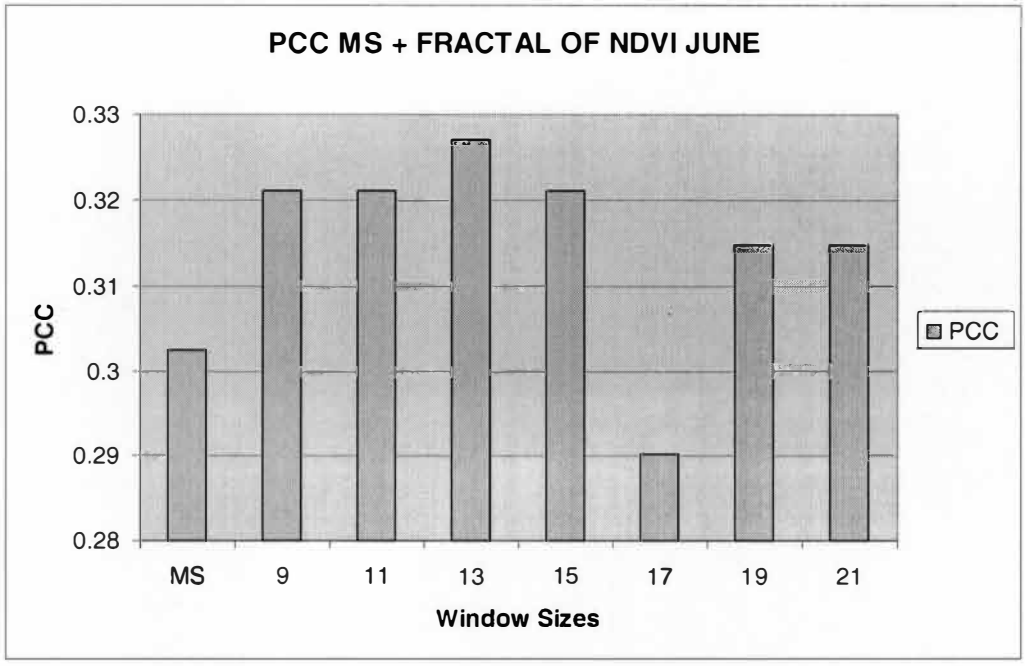

Figure 25. Percent Correctly Classified of the June Scene Using Design 4 Classification with Different Window Sizes

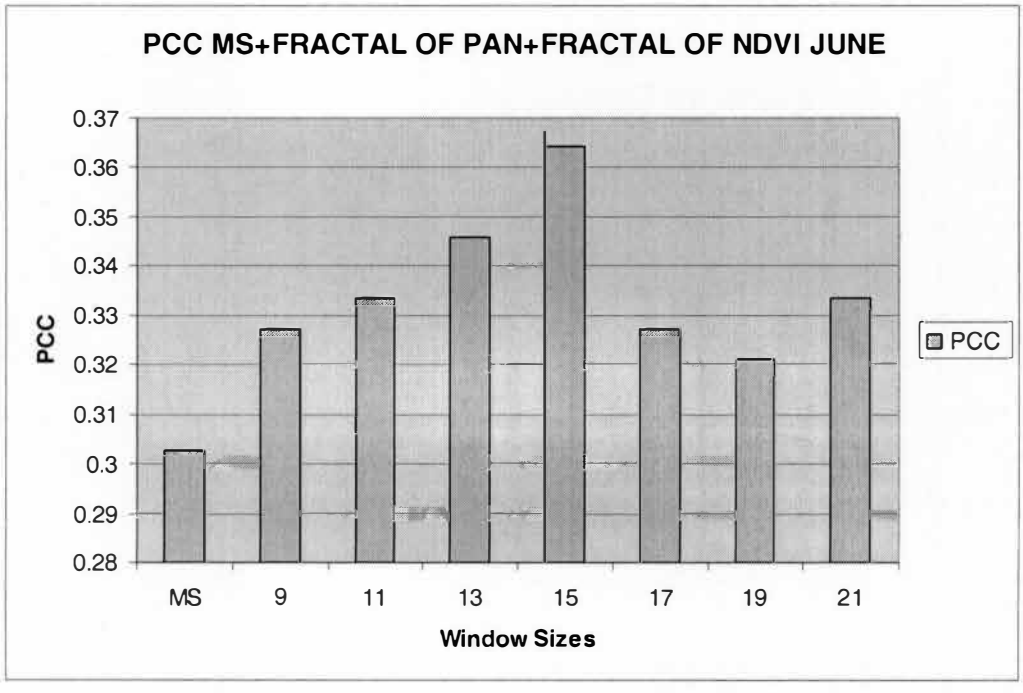

Figure 26. Percent Correctly Classified of the June Scene Using Design 6 Classification with Different Window Sizes

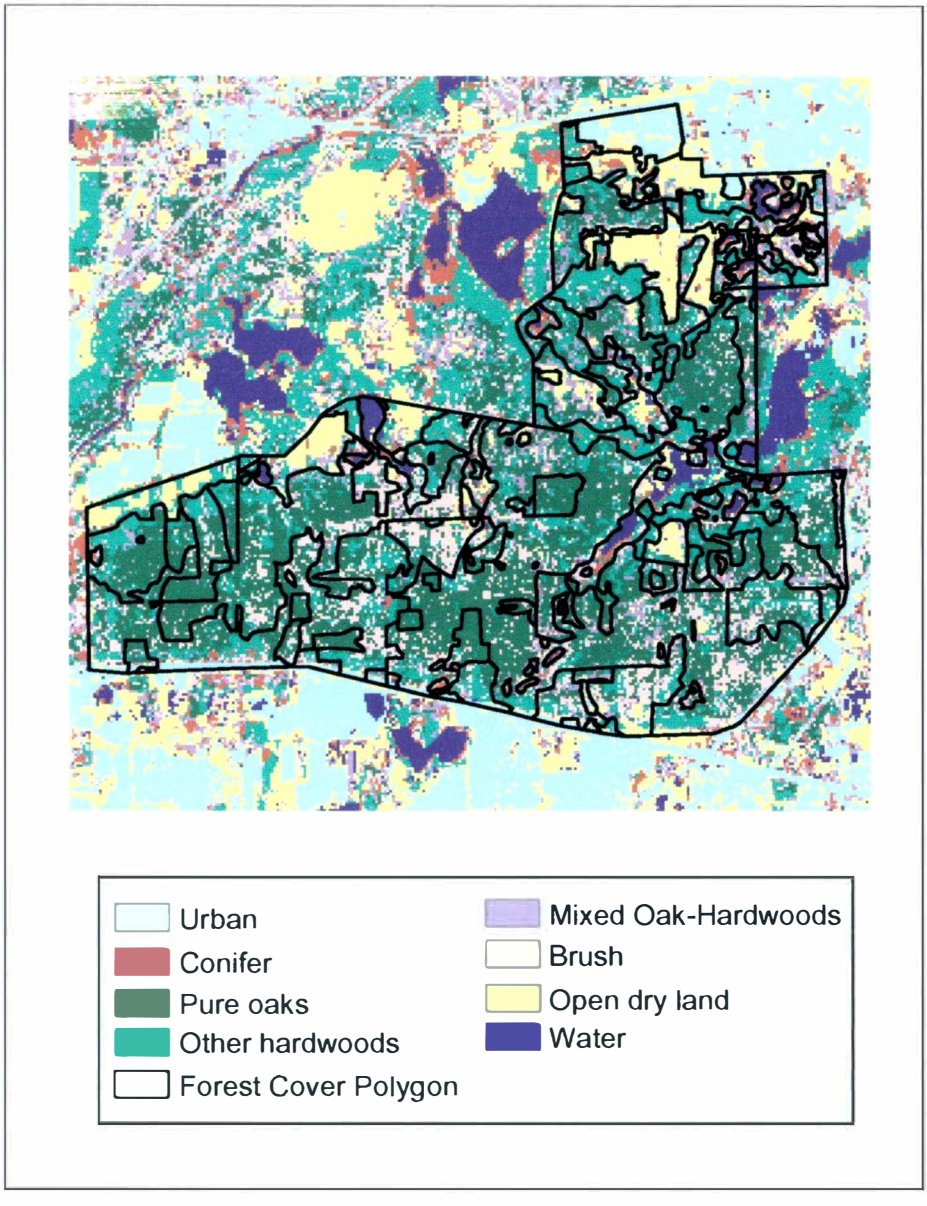

Figure 27. Classified ETM+ June Scene Using Design 6 Classification in a 15 x 15 Window

Multispectral Bands + Moran's I Measures

The addition of Moran's *I* measures in the classifications of the June scene increased the accuracy, although slightly. The Moran's *I* computed of the

Table 9. Classification Accuracy of the June Scene Using Design 6 Classification in a 15x15 Window

	Reference Data										
Class.Data	**Urban**	**Con**	**Oaks**	**Others**	**OH**	**Brush**	**ODL**	**Water**	**Tot**	**User's acc**	**Kappa**
Urban	2	0	0	1	0	2	1	0	6	33.33%	0.3165
Con	0	2	0	1	1	0	0	10	14	14.29%	0.1099
Oaks	0	3	12	14	15	2	2	5	53	22.64%	0.1416
Others	1	0	2	18	6	1	1	6	35	51.43%	0.3388
OH	0	0	1	1	4	0	4	2	12	33.33%	0.2
Brush	0	1	0	7	0	3	3	4	18	16.67%	0.1234
ODL	1	0	1	1	0	0	10	2	15	66.67%	0.617
Water	0	0	0	0	1	0	0	8	9	88.89%	0.856
Total	4	6	16	43	27	8	21	37	162		
Prod.acc	50.00%	33.33%	75.00%	41.86%	14.81%	37.50%	47.62%	21.62%			
	PCC	**Kappa**									
	36.42%	**0.2639**									

Table 10. Classification Accuracy of the October Scene Using Design 6 Classification in a 15x15 Window

		Reference Data									
Class.Data	**Urban**	**Con**	**Oaks**	**Others**	**OH**	**Brush**	**ODL**	**Water**	**Tot**	**User's acc**	**Kappa**
Urban	2	0	0	0	0	1	1	0	4	50.00%	0.4873
Con	0	3	0	2	1	0	0	1	7	42.86%	0.4066
Oaks	0	3	9	9	7	1	1	6	36	25.00%	0.1678
Others	0	0	4	24	6	3	4	9	50	48.00%	0.2921
OH	1	0	2	4	12	0	5	3	27	44.44%	0.3333
Brush	0	0	0	1	0	2	1	4	8	25.00%	0.211
ODL	1	0	1	2	1	1	9	3	18	50.00%	0.4255
Water	0	0	0	1	0	0	0	11	12	91.67%	0.892
Total	4	6	16	43	27	8	21	37	162		
Prod.acc	50.00%	50.00%	56.25%	55.81%	44.44%	25.00%	42.86%	29.73%			
	PCC	**Kappa**									
	44.44%	**0.3326**									

panchromatic image (design 3) of the June scene increased the accuracy result when used with the window of size 9x9 (33.95%, Cohen's Kappa = 0.2421); 11x11 (31.48%, Cohen's Kappa = 0.2244)); and 13x13 (31.48%, Cohen's Kappa = 0.2105).

When performed on NDVI images (design 5), the addition of Moran's *I* measurement in the classification resulted in an increased accuracy for 15x15

(30.86%, Cohen's Kappa = 0.2016); 17x17 (32.10%, Cohen's Kappa = 0.2111); 19x19 (33.33%, Cohen's Kappa = 0.2256); and 21x21 (33.95%, Cohen's Kappa = 0.2357) windows.

The use of the Moran's *I* seemed to give better result when measurements performed on both the NDVI images and panchromatic images of the June scene were added in the classification (design 7). This was true for all window sizes, where the classification accuracy improved compared to using only the spectral bands (Figure 28). The highest achievement of Moran's *I* measure was contributed by window size 17x17 and 21x21, both with the same overall accuracy and slightly different Kappa statistic (Table 11 and 12).

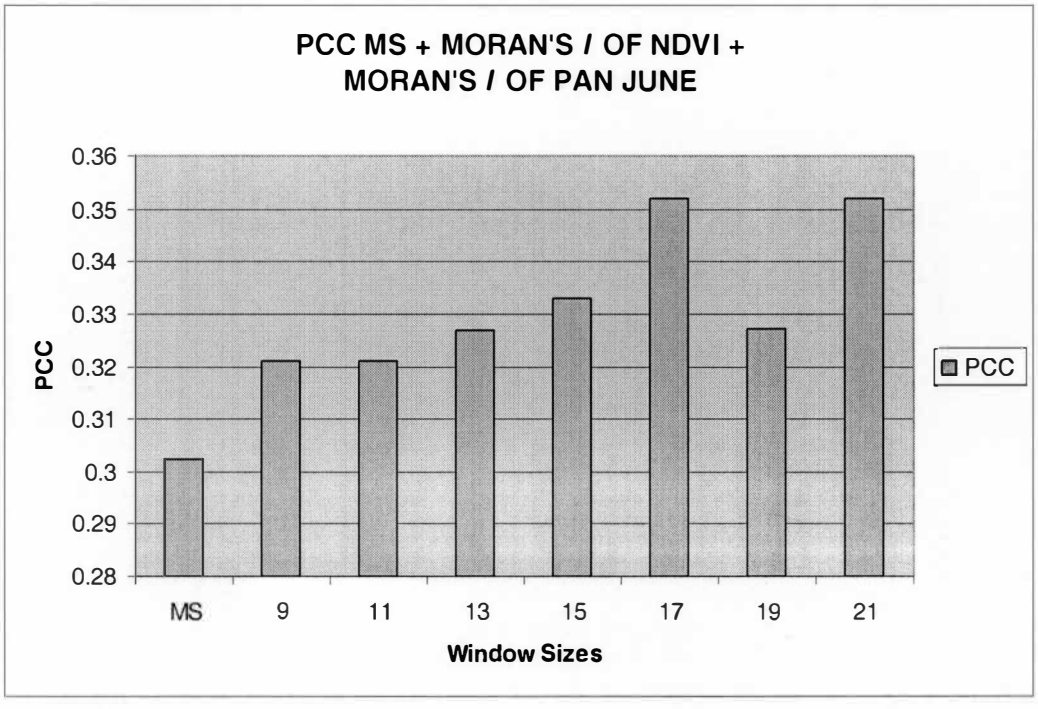

Figure 28. Percent Correctly Classified of the June Scene Using Design 7 Classification with Different Window Sizes

Table 11. Classification Accuracy of the June Scene Using Design 7 Classification in a 17x17 Window

	Reference Data										
Class.Data	**Urban**	**Con**	**Oaks**	**Others**	**OH**	**Brush**	**ODL**	**Water**	**Tot**	**User's acc**	**Kappa**
Urban	2	0	0	1	0	2	1	0	6	33.33%	0.3165
Con	0	2	0	0	2	1	0	4	9	22.22%	0.1923
Oaks	0	2	11	14	9	1	1	6	44	25.00%	0.1678
Others	1	1	2	18	10	1	3	4	40	45.00%	0.2513
OH	0	0	0	0	3	0	4	2	9	33.33%	0.2
Brush	0	1	2	8	2	3	2	11	29	10.34%	0.0569
ODL	1	0	1	0	0	0	10	2	14	71.43%	0.6717
Water	0	0	0	2	1	0	0	8	11	72.73%	0.6465
Total	4	6	16	43	27	8	21	37	162		
Prod.acc	50.00%	33.33%	68.75%	41.86%	11.11%	37.50%	47.62%	21.62%			
	PCC	**Kappa**									
	35.19%	**0.2462**									

Table 12. Classification Accuracy of the June Scene Using Design 7 Classification in a 21x21 Window

	Reference Data										
Clas. Data	**Urban**	**Con**	**Oaks**	**Others**	**OH**	**Brush**	**ODL**	**Water**	**Tot**	**User. acc**	**Kappa**
Urban	2	0	0	1	0	2	1	0	6	33.33%	0.3165
Con	0	1	0	3	2	1	1	3	11	9.09%	0.0559
Oaks	0	2	11	16	9	1	2	5	46	23.91%	0.1557
Others	1	1	2	18	7	0	2	4	35	51.43%	0.3388
OH	0	0	0	0	3	0	2	7	12	25.00%	0.1
Brush	0	2	2	4	4	4	3	8	27	14.81%	0.1039
ODL	1	0	1	0	0	0	10	2	14	71.43%	0.6717
Water	0	0	0	1	2	0	0	8	11	72.73%	0.6465
Ref Total	4	6	16	43	27	8	21	37	162		
Prod.Acc	50.00%	16.67%	68.75%	41.86%	11.11%	50.00%	47.62%	21.62%			
	PCC	**Kappa**									
	35.19%	**0.2497**									

For per-category accuracy, the other hardwoods category had an improvement in user's and producer's accuracy for all window sizes, with the addition of Moran's *I* measurement on the June panchromatic and NDVI images, compared to using the multispectral bands alone (user's accuracy of 25.58%, producer's accuracy of 37.93 %, and Cohen's Kappa value of 0.155). The highest accuracy was attained when

using the 21 x 21 window (user's accuracy of 51.43 %, producer's accuracy of 41.86%, and Cohen's Kappa value of 0.3388).

Differ from the results of the June scene, Moran's *I* measurement did not seem to help in segmenting images in the October scene, since the addition of Moran's *I* computation on both NDVI images and panchromatic images to the classification resulted in lower accuracy for all window sizes.

CHAPTER VII

CONCLUSIONS

Final Comments

The overall classification accuracies both October and June scenes were low, and the species group precision that had been desired was not met . This poor accuracy was likely caused by the similar spectral characteristics of hardwood species in the area. Even though the overall classification accuracies were still poor, the use of the combination of fractal dimension and Moran's *I* measurement with multispectral classification has a good potential to improve the accuracy of forest classification and species differentiation, since it resulted in an increase in the classification accuracies when used with certain window sizes. Table 13 and 14 summarize the results for classifications using Designs 2 – 7 with every window size, on both the June and October scenes. The '+' signs indicate accuracy improvement from using multispectral bands (MS) only (Design 1), the '- 'signs indicate no improvement, and the '++' signs show the highest accuracy on each scene.

The 19 x 19 and the 15 x 15 windows seemed to outperform the other window sizes by giving higher accuracy in most of the classification designs. For the June scene, the highest accuracy was attained by the use of fractal dimension measures on the NDVI and panchromatic image in a 15 x 15 window, combined with the multispectral bands, with an improvement of 6.17 percent (overall accuracy 36.42 percent, Cohen's Kappa value of 0.2639) as opposed to using multispectral bands

Table 13. Summary of Classifications of the June Scene

June Scene	Window Sizes						
Design	**9x9**	**11x11**	**13x13**	**15x15**	**17x17**	**19x19**	**21x21**
2 MS + Fractal of Panchromatic	+	+	+	+	+	+	+
3 MS + Moran's I of Panchromatic	+	+	+	-	-	-	-
4 MS + Fractal of NDVI	+	+	+	+	-	+	+
5 MS + Moran's I of NDVI	-	-	-	+	+	+	+
6 MS + Fractal of Panchromatic + Fractal of NDVI	+	+	+	++	+	+	+
7 MS + Moran's I of Panchromatic + Moran's I of NDVI	+	+	+	+	+	+	+

Table 14. Summary of Classifications of the October Scene

October Scene	Window Sizes						
Design	**9x9**	**11x11**	**13x13**	**15x15**	**17x17**	**19x19**	**21x21**
2 MS + Fractal of Panchromatic	+	+	+	-	-	++	-
3 MS + Moran's I of Panchromatic	-	-	-	-	-	-	-
4 MS + Fractal of NDVI	-	-	-	-	-	-	-
5 MS + Moran's I of NDVI	-	-	-	-	-	-	-
6 MS + Fractal of Panchromatic + Fractal of NDVI	-	-	-	+	-	-	-
7 MS + Moran's I of Panchromatic + Moran's I of NDVI	-	-	-	-	-	-	-

only. The highest accuracy for the October scene was achieved with the use of the fractal measure in a 19 x 19 window on the panchromatic image, combined with multispectral bands, with an improvement of 1.85 percent (overall accuracy 45.06 percent, Cohen's Kappa value of 0.3419) when compared to using multispectral bands only. The 15 x 15 and 19 x 19 windows also increased the per-category accuracy for Pure Oaks, Conifer, and Other Hardwoods category.

Future Research

For future research, several aspects may warrant further consideration. The first one is the classification scheme to be used in classifying forest composition. In establishing a classification scheme, it is important to cover all different species existing in the area. With a classification scheme that covers only Level II of the Anderson classification system, the classification accuracy would be higher but the information may not be comprehensive enough to be used in a forest management program. Modifying the classification scheme might result in different or even better classification accuracy.

The second aspect is acquisition date of the imagery being used in the study. Although it might be difficult to collect, an image taken on a specific date related to the vegetation phenology could improve the classification accuracy. In this particular study, the use of an autumn scene from approximately a week or two after October 28 may have been more useful. It would also be interesting to see the result of fractal

dimension measures on a winter image. During this leaf-off state, tree bark, stand density, and branch configuration might aid in texture measurement of the image.

The third aspect to be considered is the size of the moving window used. The window size of the texture measurement is known to affect the results. In this particular study, it was found that window sizes of 15 x 15 and 19 x 19 were superior compared to other window sizes used, however, there is still the need to find the optimal window size in texture analysis.

The fourth aspect to consider is using better ground truth with less generalization. The forest cover type map used in this study might have been too general in terms of species association categories. For instance, there are actually many non-oak tree species found in the Pure Oaks category. Better ground truth or better reference data could highly improve the classification results.

The last aspect is to consider using higher resolution data in performing forest classification such as Ikonos images, or even aerial photographs. Different tree species can be identified more easily with data that have spatial resolution higher than 30 meters. Using these data, higher classification accuracy might be achieved.

BIBLIOGRAPHY

Anderson, J.R., Hardy, E.E., Roach, J.T., and Witmer, R.A. 1976. A Land Use and Land Cover Classification System for Use with Remote Sensor Data. *Geological Survey Professional Paper 964.*

Atkinson, P.M., and Tate, N.J. 2000. Spatial Scale Problems and Geostatistical Solutions: A Review. *Professional Geographer.* 52 (4) pp. 607-623.

Arumugam, M., Emerson, C.W., Lam, N.S., and Quattrochi, D.A. 2003. Classifying Urban Land Covers Using Local Indices of Spatial Complexity. *American Society for Photogrammetry and Remote Sensing Annual Conference*, Anchorage, Alaska.

Bolstad, P. 2001. *GIS Fundamentals: A First Text on Geographic Information Systems.* Eider Press, White Bear Lake, Minnesota.

Bolstad, P., and Lillesand, T.M. 1992. Improved Classification of Forest Vegetation in Northern Wisconsin Through a Rule-Based Combination of Soils, Terrain, and Landsat Thematic Mapper Data. *Forest Science.* 38 (1) pp. 5 – 20.

Boyer, M., J. Miller, M. Belanger, and E. Hare. 1988. Senescense and spectral reflectance in leaves of northern pin oak (*Quercus palustris Muench.*). *Remote Sensing of Environment.* 25. pp. 71 – 87.

Burrough, P., and McDonnell, R. 2000. *Principles of Geographical Information System.* Oxford University Press Inc., New York.

Caird, C.P. 2001. Development of an ArcViewTM Extension to Measure Fractal Dimension. *Unpublished Master of Arts Thesis, Western Michigan University.*

Clarke, K.C. 1986. Computation of the Fractal Dimension of Topographic Surfaces Using the Triangular Prism Surface Area Method. *Computers & Geosciences.* 12 (5). pp. 713 – 722.

Cohen, J. 1960. The coefficient of agreement for nominal scales. *Educational and Psychological Measurement.* 21(1) pp. 37-46.

Congalton, R.G., and Green, K. 2001. *Assessing the Accuracy of Remotely Sensed Data: Principles and Practices.* Lewis Publisher.

Crow, T.R. 1994. Northern Lake States Late-Successional Forests: Ecological Classification and Change Detection as Guides in Ecosystem Protection and Restoration. In V.A. Sample, *Remote Sensing and GIS in Ecosystem management.* Island Press, Washington DC.

De Cola, L. 1989. Fractal Analysis of a Classified Landsat Scene. *Photogrammetric Engineering and Remote Sensing.* 55 (5). pp. 601 - 610.

Emerson, C.W.; Lam, N.S.; and Quattrochi, D.A. 1998. Multi-Scale Fractal Analysis of Image Texture and Pattern. *Photogrammetric Engineering and Remote Sensing. (*65) pp.51-61.

Emerson, C.W. 2003. A Comparison of Local Variance, Fractal Dimension, and Moran's I as Aids to Image. *The East/West Lakes Division of the American Association of Geographers Conference.* Kalamazoo, Michigan.

Environmental System Research Institute. 2002. ArcGIS 8.3 (Computer Software). Redlands, California.

ERDAS Imagine 8.6. 2001. *ERDAS Field Guide.* Leica Geosystems, GIS & Mapping Division, Georgia.

Falster, D.S. and Westoby, M. 2003. Leaf Size and Angle Vary Widely across Species: What Consequences for Light Interception? *New Phytologist.* 158. pp 509-525. Retrieved from the World Wide Web in 2003. http://www.bio.mq.edu.au/ecology/reprints/fw03newphytol.pdf

Fort Custer Training Center (FCTC). 2001. *Integrated Natural Resources Management Plan and Environmental Assessment.* Unpublished document.

Gerylo, G, Hall, R.J, Franklin, S.E, Roberts, A, Milton, F.J. 1998. Hierarchical Image Classification and Extraction of Forest Species Composition and Crown Closure from Airborne Multispectral Images. *Canadian Journal of Remote Sensing.* 24 (3). pp 219 – 232.

Gonzales, J. 1994. GIS Applications Perspective: Using Remote Sensing and GIS for Modeling Old Growth Forests. In V.A. Sample, *Remote Sensing and GIS in Ecosystem management.* Island Press, Washington DC.

Goodchild, M.F. 1980. Fractals and the Accuracy of Geographical Measures. *Mathematical Geology.* 12 (2). pp 85 – 98.

Gordon, D.K., and W.R. Philipson. 1986. A Texture-Enhancement Procedure for Separating Orchard from Forest in Thematic Mapper Data. *International Journal of Remote Sensing*. 7 (2). pp. 301 – 304.

Haralick, R.M., Shanmugan, K, and. Dinstein, I. 1973. Texture Features for Image Classification. *IEEE Trans. on System, Man, Cybernetic, SMC*-3, pp. 610-621.

Hay, G.J., Niemann, K.O., and McLean, G. 1996. An Object-Specific Image-Texture Analysis of H-Resolution Forest Imagery. *Remote Sensing of Environment*. 55. pp. 108 – 122.

Hudson, W.D. 1987. Evaluation of several classification schemes for mapping forest cover types in Michigan. *International Journal of Remote Sensing*. 8 (12). pp 1785 – 1796.

Hoffer, S.R. 1990. Non-Traditional Transformations to Aid in the Identification of Northern Hardwood Species in the Lake States. *Unpublished Master of Arts Thesis, Michigan Technological University.*

Jaggi, S., D.A Quattrochi, and N. Lam. 1993. Implementation and Operation of Three Fractal Measurement Algorithms for Analysis of Remote Sensing Data. *Computers & Geosciences*. 19 (6). pp. 745 – 767.

Jakubauskas, M.E. 1997. Effects of Forest Succession on Texture in Landsat Thematic Mapper Imagery. *Canadian Journal of Remote Sensing*. 23 (3) pp. 257 – 263.

Jensen, J.R. 2000. *Remote Sensing of the Environment. An Earth Resource Perspective*. Prentice Hall, Upper Saddle River, New Jersey.

Jensen, J.R. 1996. *Introductory Digital Image Processing. A Remote Sensing Perspective*. Simon & Schuster, Upper Saddle River, New Jersey.

Kalensky, Z., and R.R Scherk. 1975. Accuracy of forest mapping from Landsat Computer Compatible Tapes. *Proceedings of the 10th International Symposium on Remote Sensing of Environment*, 6 – 10 October (Ann Arbor, Michigan), pp. 1159 – 1167.

Keller, J.M., Chen, S., and Crownover, R.M. 1989. Texture Description and Segmentation through Fractal Geometry. *Computer Vision, Graphics, and Image Processing*. 45, pp. 150 – 166.

Lam, N., and D.A. Quattrochi. 1992. On the Issues of Scale, Resolution, and Fractal Analysis in the mapping Sciences. *Professional Geographer*. 44 (1). pp 88 – 98.

Lam, N., and L. De Cola. 1993. *Fractals in Geography*. PTR Prentice Hall, New Jersey.

Lam, N., H. Qiu, D.A. Quattrochi, C.W, Emerson. 2002. An Evaluation of Fractal Methods for Characterizing Image Complexity. *Cartography and Geographic Information Science*. 29 (1). pp. 25-35.

Leica Geosystem. 2002. ERDAS Imagine 8.6 (Computer Software). Atlanta, Georgia.

Lillesand, T.M., and Kiefer, R.W. 2000. *Remote Sensing and Image Interpretation, Fourth Edition*. John Wiley and Sons.

MacDonald, G. 2003. *Biogeography. Introduction to Space, Time, and Life*. John Wiley and Sons.

Mandelbrot, B. 1977. *Fractals Form, Chance, and Dimension*. W.H. Freeman and Company, San Francisco

Mandelbrot, B. 1982. *The Fractal Geometry of Nature*. W.H. Freeman and Company, San Francisco.

Michigan Department of Natural Resources. 2003. *Michigan Timberland Highlights*. Retrieved from the World Wide Web in 2003. http://www.michigan.gov/dnr/0,1607,7-153-10367-33944--,00.html

Mladenoff, D.J., and G.E. Host. 1994. Ecological Perspective: Current and Potential Applications of Remote Sensing and GIS to Ecosystem Analysis. In V.A. Sample, *Remote Sensing and GIS in Ecosystem management*. Island Press, Washington DC.

Moskal, L.M., and S.E Franklin. 2001. Classifying Multilayer Forest Structure and Composition Using High Resolution, Compact Airborne Spectrographic Imager Image Texture. *American Society of Remote Sensing and Photogrammetry Annual Conference*, April (St. Louis, Mississipi).

Moskal, L.M., and M.E Jakubauskas. 2001. Discriminating Forest Stand Age Classes Using 2nd Order Image Texture in the Central Plateau of Yellowstone National Park. *The 4th International Forestry and Agricultural Remote Sensing Conference and Exhibition,* November (Denver, Colorado).

National Community Forestry Center Northern Forest Region (NCFCNFR). 2003. Glossary of Forest-Related Terms. Retrieved from the World Wide Web in 2003. http://www.ncfcnfr.net/glossary.html

National Climatic Data Center. 2003. Time Series Archive: US Precipitation and Temperatures in 2000. Retrieved from the World Wide Web in 2003. http://lwf.ncdc.noaa.gov/oa/climate/research/2000/CMB_prod_us_tempandprcp.html

Quattrochi, D.A., Lam, N., Qiu, H., and Zhao, W. 1997. Image Characterization and Modeling System (ICAMS): A Geographic Information System for the Characterization and Modeling of Multiscale Remote Sensing Data. In D.A. Quattrochi and M.F. Goodchild, *Scale in Remote Sensing and GIS*. CRC Lewis, Florida.

Quattrochi, D.A., C.W. Emerson, N. S. Lam, and H. Qiu. 2001. Fractal Characterization of Multitemporal Remote Sensing Data. In N.J Tate and P.M. Atkinson, *Modelling Scale in Geographic Information Science.* John Wiley and Sons.

Rauscher, H.M. *Importance of Oaks*. USDA Forest Service. Retrieved from the World Wide Web in 2003. http://www.forestryencyclopedia.net/index.html?targetId=42&&anchorId=27

Rogerson, P.A. 2001. *Statistical Methods for Geography.* Sage Publications.

Roller, N.E., and L. Visser. 1980. Accuracy of Landsat Forest Cover Type Mapping in the Lake States region of the United States. *The 14th International Symposium on Remote Sensing of Environment* , 23 – 30 April (San Jose, Costa Rica).

Schriever, J.R., and R.G Congalton. 1993. Mapping forest cover-types in New Hampshire using Multi-Temporal Landsat Thematic Mapper Data. *American Society of Remote Sensing and Photogrammetry Annual Conference /ACSM Annual Convention & Exposition*, 15 – 19 February (New Orleans, Lousiana), pp. 333 – 342.

Smith, N.F. 2002. *Trees of Michigan and the Upper Great Lakes.* Thunder Bay Press, Michigan.

The International Ecotourism Community. 2003. Retrieved from the World Wide Web in 2003. http://www.ecotourism.org/

Virkkala,R. 1993. Ranges of Northern Forest Passerine: A Fractal Analysis. *OIKOS*. 67. pp. 218-226.

Wilson, C.P. 1997. Discrimination of Hardwood Species in Michigan's Northern Lower Peninsula Using Winter Landsat ThematicMapper Data. *Unpublished Master of Arts Thesis, Eastern Michigan University.*

Wolter, P., D.J Mladenoff, G.E Host, and T.R Crow. 1995. Improved Forest Classification in the Northern Lake States Using Multi-Temporal Landsat Imagery. *Photogrammetric Engineering & Remote Sensing*. 61 (9). pp 1129 – 1143.

Xia, Zong-guo and Clarke, K. C. 1997. Approaches to Scaling of Spatial Data in the Geosciences. In D. A Quattrochi and M Goodchild. *Scaling of Remote Sensing Data For GIS*. CRC Lewis, Florida.

Zeide, B. 1991. Fractal Geometry in Forestry Application. *Forest Ecology and Management*. 46 (3-4). pp. 179-188

Zhu, Q.J., Rong T.Z., and Sun, R. 2000. A Case Study on Fractal Simulation of Forest Fire Spread. *Science in China*. E 43 104-U2.